CHALMERS

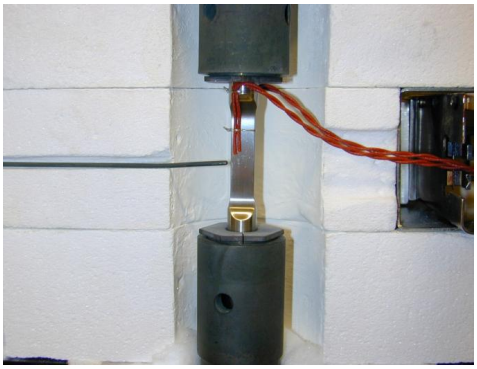

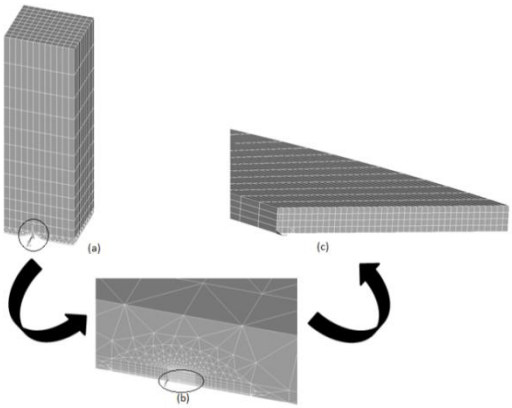

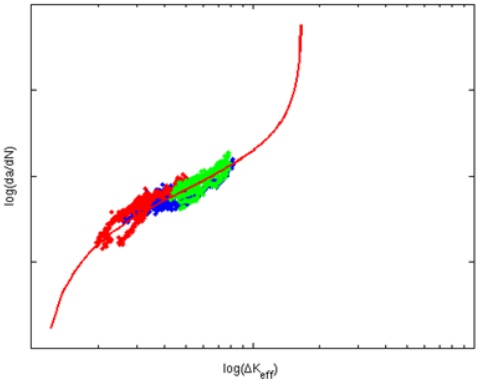

A Combined Numerical and Statistical Approach to Crack Propagation Modeling and Prediction of Crack Propagation Rates

Master's Thesis in Applied Mechanics

MARTIN REMBECK
ANDERS SJÖBLOM

Department of Applied Mechanics
Division of Material and Computational Mechanics
CHALMERS UNIVERSITY OF TECHNOLOGY
Göteborg, Sweden 2012
Master's thesis 2012:32

MASTER'S THESIS IN APPLIED MECHANICS

A Combined Numerical and Statistical Approach to Crack Propagation Modeling and Prediction of Crack Propagation Rates

MARTIN REMBECK

ANDERS SJÖBLOM

Department of Applied Mechanics
Division of Material and Computational Mechanics
CHALMERS UNIVERSITY OF TECHNOLOGY
Göteborg, Sweden 2012

A Combined Numerical and Statistical Approach to Crack Propagation Modeling and Prediction of Crack Propagation Rates

MARTIN REMBECK

ANDERS SJÖBLOM

Master's Thesis 2012:32
ISSN 1652-8557
Department of Applied Mechanics
Division of Material and Computational Mechanics
Chalmers University of Technology
SE-412 96 Göteborg
Sweden
Telephone: + 46 (0)31-772 1000

Cover:
Picture of the crack propagation set-up at Volvo Aero (top), overview of the numerical model (left), and curve fitting to experimental data (right).

Chalmers Reproservice
Göteborg, Sweden 2012

A Combined Numerical and Statistical Approach to Crack Propagation Modeling and Prediction of Crack Propagation Rates
Master's Thesis in Applied Mechanics
MARTIN REMBECK, ANDERS SJÖBLOM
Department of Applied Mechanics
Division of Material and Computational Mechanics
Chalmers University of Technology

ABSTRACT

In order for the engineer to correctly predict the operational life of a component it is important to understand the physical background to fatigue, i.e. the growth of fatigue cracks. In the industry, the dominating models used for crack propagation analyses use are based on either a pure curve fit procedure or models that intend to capture the physical phenomenon related to the crack growth. The present thesis project attempts to make more accurate life predictions of aircraft engine components by employing a more physical approach to crack propagation modeling. In particular, the thesis deals with the derivation of five parameters in the NASGRO® equation for crack growth. Four of these parameters were derived by curve fitting to experimental data and one parameter, the crack closure, was derived by finite element analysis. This differs from the empirical method, currently in industrial use, determining life where all five parameters are obtained from curve fitting. Both methods were evaluated and compared to experimental data for cast Inconel 718 using statistical tools. The crack closure, here assumed to be induced by plasticity, was determined by numerical simulations of fatigue crack growth of a semi-circular surface crack in a 3D domain. The objective was to obtain an unequivocal value of Newman's plane stress/strain constraint factor, α, which is directly related to the closure level. In this study experimental data of cast Inconel 718 test specimens at different temperatures, and for three *R*-ratios, was utilized. The numerical analysis used a kinematic multi-linear hardening constitutive model and crack propagation was modeled by releasing all nodes at the crack front after unloading in a one-node-per-one-cycle debonding scheme. Different values of the plane stress/strain constraint factor were found for each of the three R-ratios, i.e. an unequivocal value was not obtained and instead an average was used. The predicted lives were calculated by use of the established parameters in the NASGRO® equation and were compared to the actual lives observed in the experimental testing. The proposed method gave similar results as to the empirical pure curve fit method, although the models credibility is increased due to the better understanding of the crack closure phenomenon. Hence, the model can be expanded for different geometries with different crack closure levels resulting in more accurate life predictions. Consequently, the thesis provides a basis for further improvements of the crack propagation modeling.

Key words: Fatigue crack propagation, Crack closure, NASGRO®, Finite Element Analysis

Contents

Preface

This is a Master's Thesis under the Department of Applied Mechanics at Chalmers University of Technology. The thesis was carried out at Volvo Aero India (VAI) in Bangalore, India, in collaboration with the Division of Material and Computational Mechanics at Chalmers University of Technology.

Professional assistance has been obtained from both Volvo Aero and Chalmers. Many thanks to our supervisors Dr. Tomas Månsson and Dr. Sushovan Roychowdhury from Volvo Aero and Prof. Lennart Josefson (examiner) and Doc. Anders Ekberg from Chalmers, whose assistance has been invaluable.

We also would like to send special thanks to Mr. Thomas Gustafsson and Doc. Robert Lundberg at Volvo Aero who made this project possible and enabled this amazing trip to India.

Last by not least we want to thank Asim Rashid and all the employees at VAI, who have given us enormous support during our stay, not only regarding the actual project but also regarding challenges in our everyday lives.

Namastē!

Bangalore, June 2012

Martin Rembeck and Anders Sjöblom

Notations

Notation	*Unit*	*Description*
R	[-]	Stress ratio
T	[^{o}C]	Temperature
K	[MPa$\sqrt{\text{mm}}$]	Stress intensity factor, predicting the stress intensity at the crack tip
K_{max}	[MPa$\sqrt{\text{mm}}$]	Maximum stress intensity factor
K_{min}	[MPa$\sqrt{\text{mm}}$]	Minimum stress intensity factor (may also be negative)
ΔK	[MPa$\sqrt{\text{mm}}$]	Stress intensity range
ΔK_{eff}	[MPa$\sqrt{\text{mm}}$]	Effective stress intensity range
ΔK_{th}	[MPa$\sqrt{\text{mm}}$]	Threshold stress intensity range
K_c	[MPa$\sqrt{\text{mm}}$]	Material fracture toughness
K_{op}	[MPa$\sqrt{\text{mm}}$]	Stress intensity factor at crack opening
K_{cl}	[MPa$\sqrt{\text{mm}}$]	Stress intensity factor at crack closure
f	[-]	Crack opening function
α	[-]	Plane stress/strain constraint factor
σ_{max}	[MPa]	Maximum stress
σ_y	[MPa]	Material yield strength
σ_u	[MPa]	Material ultimate strength
σ_0	[MPa]	Material flow stress
ε_p	[-]	Plastic strain
r_p	[mm]	Plastic zone size
L_e	[mm]	Element length ahead of crack tip in the in propagating direction
φ	[-]	Angle in the circumferential direction in the crack plane
t	[mm]	Specimen thickness
W	[mm]	Specimen width
H	[mm]	Specimen height
a	[mm]	Crack width
c	[mm]	Crack length
Δa	[mm]	Crack propagation increment
da/dN	[mm/cycle]	Crack growth per cycle
C	[-]	Constant in NASGRO® equation
n	[-]	Constant in NASGRO® equation
p	[-]	Constant in NASGRO® equation
q	[-]	Constant in NASGRO® equation

1 Introduction

This master's thesis deals with crack propagation modeling, in particular the derivation of five parameters in the NASGRO® equation. The crack closure level, which is one of these parameters, is determined by means of numerical simulations of fatigue crack growth and the other four parameters are determined by a least square fit to experimental data. Further, the thesis aims to compare this model to Volvo Aero Corporations (VAC) current method for determining fatigue life. In their method the closure level is not numerically calculated nor found experimentally, instead it is derived by curve fitting. Hence, this thesis provides a deeper physical understanding of the crack propagation behavior. This chapter gives a further introduction to the thesis with focus on presenting relevant background and methods to solve the problem.

1.1 Background

It is important to understand the fatigue phenomenon in order for the engineer to correctly predict the operational life for any construction and material. Fatigue crack growth is often described by semi-empirical equations, many of which contain a large amount of material, geometry and load related parameters. Some equations describe only specific parts of the crack growth life, such as the Paris law [1] which is limited to the crack growth in the linear part of the logarithmic relationship between crack propagation rate and stress intensity range. At VAC the NASGRO® equation is used to describe the entire crack growth life. In this model the *R*-ratio correction is modeled by assuming that a crack closure function is applicable. The crack closure is based on plasticity induced crack closure (PICC), which is possible to calculate with finite element models (FE-models), and is important to determine since it influences the crack propagation rate.

It is often difficult and expensive to identify all necessary information about the actual material to determine all parameters in a complex model such as the ones describing the crack propagation rate. For this reason the uncertainties in predicted fatigue lives may become very large. The scatter in fatigue lives can also be seen as due to the fact that fatigue is a local phenomenon. The crack is initiated (or pre-existing) where there are stress concentrations due to microstructural inhomogeneities, grain structure influences and/or other influences at micro- or macro scale. This happens even under very controlled loading conditions and in a very controlled environment with specimens cut from the same sheet.

The dominating material models used for crack propagation analyses are based on either a pure curve fit procedure or models that intend to capture some physical phenomenon related to them. In the first case a series of experiments are carried out and models, such as the Walker model, is used and all parameters are obtained through curve fit. The other type of models has some physical explanation to limited known phenomenon. Both of the "modeling classes" are likely to give similar accuracy, at least for average crack propagation rates. The applicability of the models used will be evident when the material scatter is to be estimated which is useful for probabilistic analyses (i.e in determining safety factors or when risk of failure is to be calculated). A "poor" model may give an unrealistic material scatter. In the case of NASGRO® equation the closure level is currently determined at VAC by using a least square fit procedure. The curve fitting process results in different closure levels for different temperatures for the same *R*-ratio, which is unexplained. An alternate way to compute the closure level is through FE analysis. This approach belongs to the second type of material model discussed above. However, FE-modeling of the closure level compared to the simplified closure models available in NASGRO® needs to be evaluated before adopting it as a regular process.

It is known that crack propagation rates may differ for different crack geometries (surface flaws vs. through cracks). One reason for such discrepancy may be different closure levels. A firm understanding of the available model may allow for expanding the model to different geometries and therefore result in more accurate predictions. Finally, assuming an erroneous constraint parameter in the simplified closure model (NASGRO® model) may give unrealistic closure response should load interaction effects be taken into account.

1.2 Objective

This study uses experimental data of cast Inconel 718 test specimens with a semi-circular surface crack at different temperatures and for three different *R*-ratios. The first part of the thesis handles numerical calculations of crack closure levels for the *R*-ratios and temperatures for which the crack propagation test results are derived from. The finite element (FE) calculated closure levels are used to remove the *R*-ratio dependence from the experimental tests and thus provide means to evaluate an effective (*R*-ratio independent) stress intensity factor.

The goal is to obtain an unequivocal value of the plane stress/strain constraint factor, α, which is directly related to the closure level. Previous studies have shown that the free surface of the crack resembles plane stress behavior, and the mid-plane resembles plane strain [2] (see Figure C.2 in Appendix C for illustration). This also affects the level of closure, and it has been seen that the crack closes earlier at the surface than at the mid-plane. A 3D analysis is obviously necessary to capture the variation of the crack closure level at the crack front.

The second part of the thesis deals with statistical modeling of propagation rates. With the closure level established from FEA the four remaining unknown parameters *C*, *n*, *p*, *q* in the NASGRO® equation will be determined by a least square fit to experimental data.

The outcome of the thesis is:

1) FE-model to predict closure levels for surface cracks leading to an unequivocal value of the parameter, α.
2) Established values of the parameters *C*, *n*, *p* and *q* based on a least square fit to experimental data.
3) An evaluation of the proposed analysis to the method currently used at VAC for predicting lives.

1.3 Method

To describe crack propagation in the test specimens, already established and accepted fatigue theories are used. In particular the NASGRO® equation, which is an empirical model describing the entire crack growth curve from low to high ΔK, is adopted. For the numerical calculations for establishing the closure levels, the commercial software ANSYS, which is commonly used at VAC, is employed. Further, MATLAB and Excel are used for pre- and post-processing of the data. The crack propagation analysis is done in the NASGRO® software for its simplicity. Further, it is the tool currently used at VAC. Evaluation of the methods are performed by comparing the actual and predicted lives for a number of cases tested in the material lab at VAC.

1.4 Limitations

Several simplifications are obviously needed in the numerical analysis, which is covered in section 3. General limitations of work presented in the thesis include:

- Crack closure mechanisms other than plasticity-induced crack closure are not considered.
- The numerical analysis is only used to establish crack closure levels and not to simulate the actual fatigue crack propagation rate.

2 Theory

This chapter describes the fundamentals of fatigue crack growth and the equations related to this theory. The phenomenon of crack closure is especially important and is carefully described. One particular equation of interest is the NASGRO® equation which is explained in detail below including some remarks on the use of the NASGRO® software.

2.1 Physical description

Experiments of crack propagation during cyclic loading reveals striation on the fracture surface of ductile materials. The striations represent the increment of growth occurring in one load cycle, which reflect the operation of slip planes at a crack tip causing plastic blunting and sharpening. During reverse loading compressive stresses at the crack tip reverse slipping, but the newly created surface cannot be removed by reconnection of the atomic bonds. At cyclic loading, as the crack propagates, a plastic wake is formed behind the crack tip and will induce crack closure.

If the plastic zone at the crack tip is sufficiently small compared to other length scales, such that it is embedded in the elastic singularity zone, the condition at the crack tip is uniquely defined by the current stress intensity [3]. The typical fatigue crack growth behavior in metals is illustrated Figure 2.1, showing the logarithmic relationship between crack propagation rate and stress intensity range. The curve

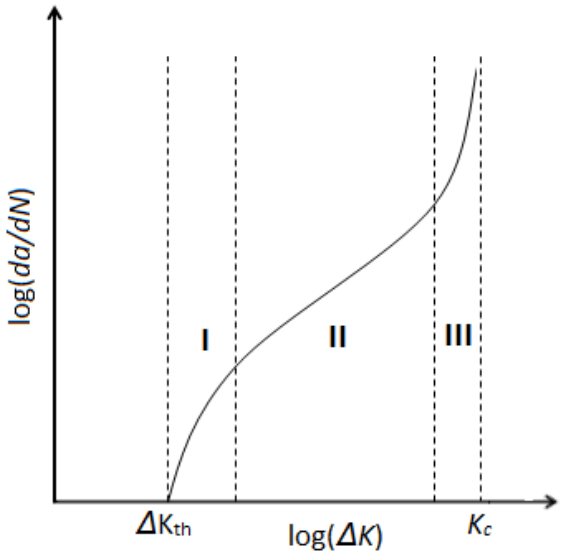

Figure 2.1: Typical fatigue crack propagation behavior in metals, showing the logarithmic relationship between crack propagation rate (*da/dN*) and stress intensity range (Δ*K*).

consists of three distinct regions. Below a threshold ΔK_{th}, *da/dN* approaches zero and the crack will not grow. In the intermediate part a linear trend is evident. At high ΔK-values the crack growth rate escalates rapidly as the stress intensity factor increases towards a critical value K_c, the fracture toughness of the material. The crack growth can, under small scale yielding condition (SSY), be defined in a general form as:

$$\frac{da}{dN} = f(\Delta K, R) \tag{2.1}$$

where:

$$\Delta K = K_{\max} - K_{\min} \tag{2.2}$$

$$R = \frac{K_{\min}}{K_{\max}} \tag{2.3}$$

$$\frac{da}{dN} = crack\ growth\ per\ cycle \tag{2.4}$$

A number of equations have been developed similar to this form, most of which are empirical, describing both short and long cracks. Paris and Erdogan [4] were the first to establish an equation of such a form. This equation, called Paris law, only describes the linear part of the logarithmic relationship between crack propagation rate, *da/dN*, and stress intensity range, ΔK. Once the crack growth law is determined the equation can be integrated to compute the operational life of a component, given a critical crack size and a fracture criterion. The parameters that influence the crack growth rate are the loading conditions, component geometry, material and its microstructure, temperature and environment.

2.1.1 Crack closure[1]

Several mechanisms can cause crack closure such as plasticity induced crack closure (PICC), roughness induced closure which is influenced by microstructure and oxide induced crack closure which is associated with an aggressive environment, among others [5]. The roughness induced crack closure is related to the crack path deflection, and is especially pronounced at relatively low crack growth rates [6]. PICC is dominant over a broad range of stress intensity or at relatively high crack growth rates [7]. Only PICC will be studied in this thesis.

The PICC level is a complex relation between plastic strains occurring in the vicinity of the crack tip and the growth of the crack through this plastically deformed material. As the crack propagates it leaves behind a plastic wake, see Figure 2.2. The residual stretch in the plastic wake brings forth the crack surface to close at the tip at a certain fraction of the maximum load. Elber was the first to discover crack closure at tensile loading [3] and suggested that the crack tip deformation and crack propagation rate are controlled by an effective stress intensity range, ΔK_{eff}, defined by:

[1] Usually most authors do not distinguish between crack closure and crack opening, which may cause some confusion. In this report the mix of the terms is strived to be avoided, however depending on the context one or the other term is more suitable to use. See also chapter 3.2.4 for further discussion.

$$\Delta K_{\text{eff}} = K_{\max} - K_{\text{op}} \tag{2.5}$$

Here K_{op} is the stress intensity factor corresponding to the case when the crack surface is completely opened. Following Elber [7], ΔK can be replaced by ΔK_{eff} in equation (2.1) and the crack growth rate can now be expressed as:

$$\frac{da}{dN} = C(\Delta K_{\text{eff}})^n \tag{2.6}$$

Where C and n are material parameters and are derived empirically.

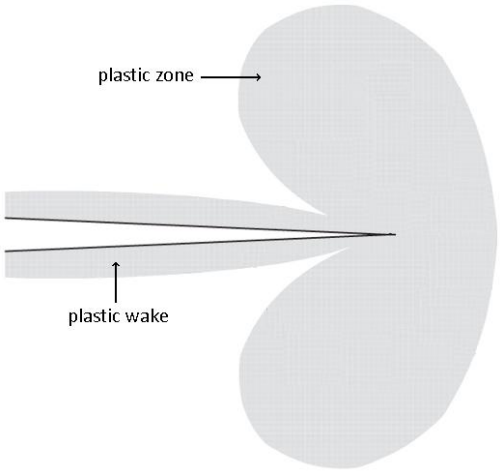

Figure 2.2: The forward plastic zone (plastic zone at maximum loading) at a crack tip and the plastic wake formed after some growth.

It is especially important to understand how to model the plastic zone in a physically sound, although simplified, manner. The remote surrounding that encloses the plastic zone can still be modeled as linear-elastic and linear elastic fracture mechanics (LEFM) is applicable in describing the crack loading if the plastic zone is sufficiently small compared to other length scales. Such conditions are known as small-scale yielding (SSY) and are presumed in this thesis; these conditions are illustrated in Figure 2.3. The

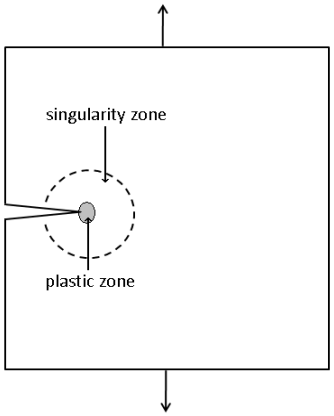

Figure 2.3: Small scale yielding (SSY) conditions.

stress state in the plastic zone is dependent on the size of the plastic zone, if it is small compared to the thickness, plane strain conditions exists. If the plastic zone is of the same magnitude as the thickness the state of stress is mainly plane stress. When examining the crack closure during unloading it can be observed that the crack closes faster on the free surface as compared to the mid-plane. At the surface the stress condition can be described by plane stress, because the plastic deformations are less constrained on the free surface. However towards the center of the component the stress condition is best described by plane deformation since the plastic deformations are constrained. In between, there is a transition zone which can neither be described by plane stress nor plane strain. A 3D analysis is obviously necessary to capture the variation of the crack closure level at the crack front, and crack closure is therefore indeed a 3D phenomenon.

2.2 Threshold stress intensity range, ΔK_{th}

The threshold stress intensity range, ΔK_{th}, is the point below which a macroscopic crack does not grow. The threshold is generally believed to consist of two components [2]: an intrinsic threshold that is a material property, and extrinsic threshold which is a function of different loading variables, e.g. the *R*-ratio. In general, the *R*-ratio has a strong effect on the behavior at low crack growth rates, and thereby also the threshold level [1]. It is generally believed that the *R*-ratio effect on the threshold level is related to crack closure, however scientists have diverging theories on this matter. The threshold level may also be very dependent on the environment, e.g. different values can be found for air and vacuum, even though air is not considered to be a very corrosive environment [2]. In summary, the threshold stress intensity range is a very complex parameter, which is not yet fully understood. There are also difficulties when experimentally determining it, which makes crack growth rate predictions especially hard in this region.

2.3 NASGRO® equation

The NASGRO® equation (2.7) is an extension of equation (2.6) and describes the entire crack growth life, taking account of both the threshold stress intensity range, ΔK_{th} , and the material fracture toughness, K_{c} [2]. The crack propagation rate is evaluated from the stress intensity factor range, ΔK, the *R*-ratio, threshold levels and fracture toughness. The equation is given by:

$$\frac{da}{dN} = C\left[\left(\frac{1-f}{1-R}\right)\Delta K\right]^{n} \frac{\left(1-\frac{\Delta K_{\mathrm{th}}}{\Delta K}\right)^{p}}{\left(1-\frac{K_{\max}}{K_{\mathrm{c}}}\right)^{q}} \tag{2.7}$$

where *C*, *n*, *p* and *q* are empirically derived parameters.

The crack opening function is defined as $f = \frac{K_{\mathrm{op}}}{K_{\max}}$. In this thesis it will, as mentioned earlier, be determined numerically by using finite element analysis.

Newman [8] suggested that crack closure is a function of the stress ratio, as well as the stress-state and the maximum stress level, $\sigma_{\max}$. He defined the crack opening function, *f*, as:

$$f = \frac{K_{\mathrm{op}}}{K_{\max}} = \begin{cases} \max(R, A_0 + A_1 R + A_2 R^2 + A_3 R^3), & R \geq 0 \\ A_0 + A_1 R, & -2 \leq R < 0 \end{cases} \tag{2.8}$$

where the polynomial coefficients are given by:

$$A_0 = (0.825 + 0.34\alpha + 0.05\alpha^2)\left[\cos\left(\frac{\pi}{2}\frac{\sigma_{\max}}{\sigma_0}\right)\right]^{\frac{1}{\alpha}} \quad (2.9)$$

(where $1 < \alpha < 3$ and $0 < \frac{\sigma_{\max}}{\sigma_0} < 1$)

$$A_1 = (0.415 - 0.071\alpha)\frac{\sigma_{\max}}{\sigma_0} \quad (2.10)$$

$$A_2 = 1 - A_0 - A_1 - A_3 \quad (2.11)$$

$$A_3 = 2A_0 + A_1 - 1. \quad (2.12)$$

The parameter, α, is the plane stress/strain constraint factor and $\frac{\sigma_{\max}}{\sigma_0}$ is the ratio between maximum stress and the material flow stress. The material flow stress is usually defined as the average between the material yielding and ultimate strength [9], and the same definition is used in this thesis:

$$\sigma_0 = \frac{\sigma_y + \sigma_u}{2} \quad (2.13)$$

The plane stress/strain constraint factor, α, is considered as a constant with a value ranging from 1 (plane stress) to 3 (plane strain). Figure 2.4 below shows the crack opening function, f, versus stress ratio, R, by applying equation (2.8) for different values of (a) α and (b) $\frac{\sigma_{max}}{\sigma_0}$.

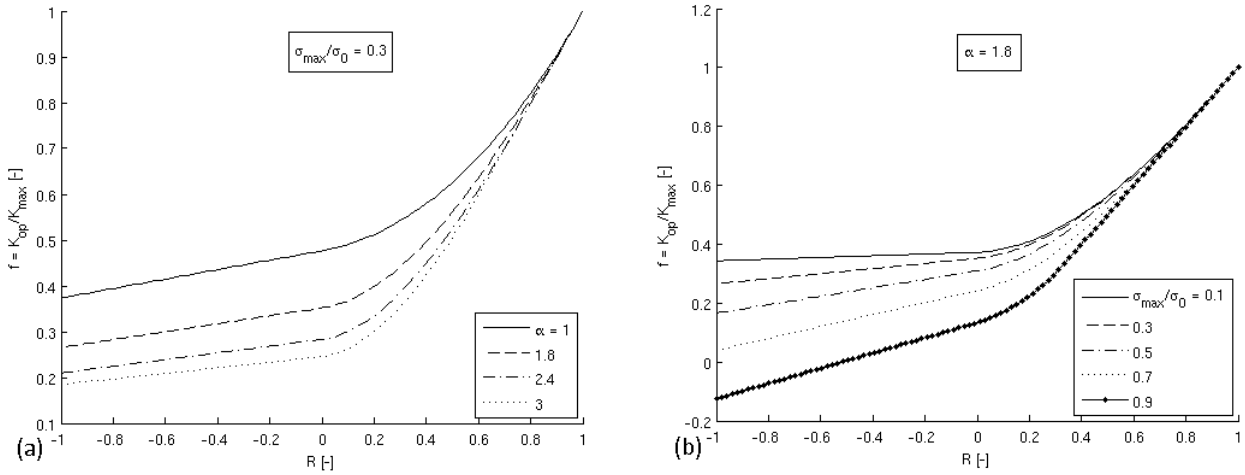

Figure 2.4: Crack opening function, f, versus stress ratio, R, for different values of (a) α $\left(\frac{\sigma_{max}}{\sigma_0} = 0.3\right)$ and (b) $\frac{\sigma_{max}}{\sigma_0}$ $(\alpha = 1.8)$.

It is obvious that both the plane stress/strain constraint factor and the maximum stress level have a significant effect on the crack opening function. In the NASGRO® software the opening function, f, is not given explicitly. The user instead has to specify α and $\frac{\sigma_{\max}}{\sigma_0}$. Figure 2.5 below shows the plane

stress/strain constraint factor, α, versus crack opening function, *f*, for *R* = 0 and for two different values of $\frac{\sigma_{\max}}{\sigma_0}$.

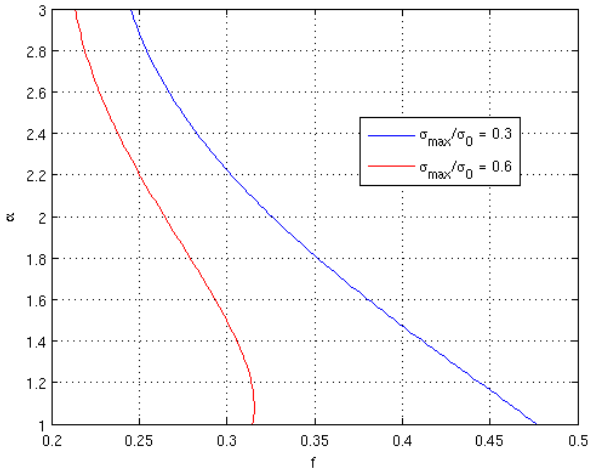

Figure 2.5: Plane stress/strain constraint factor, α, versus crack opening function, f, for (a) $\frac{\sigma_{max}}{\sigma_0} = 0.3$ and (b) $\frac{\sigma_{max}}{\sigma_0} = 0.6$.

An important observation is that *f* has a much wider range of values for the low load ($\sigma_{max}/\sigma_0 = 0.3$), i.e. an increase in applied load has a constraining effect on *f*. The numerically established *f*, the loading condition giving σ_{max} and material property σ_0 is used to solve for α by means of Newman's crack opening function.

3 Finite element analysis to determine crack closure levels

Crack closure is the contact of crack surfaces during a portion of the load cycle. It is often hard to determine the crack closure level and one approach is to find it numerically. Experimental techniques provide only average values for crack closure [10], but with a numerical approach, such as a finite element (FE) analyses, the 3D effects are easy to find. A 3D analysis will provide an understanding of how the closure level varies along the crack front of a Kb-specimen and the potential to describe crack closure, and thereby α, with only one value for such a geometry. In this work the crack closure, of a surface crack, induced by plasticity, along a 3D crack front has been simulated for different R-ratios and temperatures. A careful design of the FE-model and the numerical crack propagation scheme is essential for accurate crack closure results and an investigation of current research has been performed.

A fundamental aspect in the FE analyses is to capture the cyclic elastic-plastic behavior of the material, this is especially important when unloading occurs. Material test results, produced by VAC, for the cyclic behavior is used to model hardening. The accuracy for crack propagation analysis of the FE-model is deeply associated with the mesh; it depends primarily on the type and size of the elements near the crack tip. An intense mesh refinement is performed around the crack front in order to accurately compute the strong gradient of the stress field. A coarse mesh far from the crack is necessary to save computational time. Roychowdhury and Dodds [11, 12] and other researchers suggest a modeling condition concerning the number of elements in front of the crack tip. A certain number of elements should be contained within the initial forward and reversed plastic zones. However, larger element size can be allowed depending on the order of element [10]. The element size at and around the crack tip also determines the total number of elements needed in the model and smallest crack increment during growth.

The crack is propagated by releasing all nodes along the crack front by increments of one element (Δa) per load cycle. The nodes are released by removing the symmetry boundary conditions imposed on them. The set of nodes is released after unloading and opening and closure levels are calculated for every load cycle when the first node behind the crack tip loses/comes into contact. The crack is extended until the steady state is reached where stabilized values of the closure levels are obtained. Attaining steady state condition determines total number of load cycles simulated. Aspects of importance for the crack propagation scheme can be summarized:

- Crack tip node release scheme – at what point in the cycle growth occurs (section 3.2.1.)
- Number of load cycles per node release (section 3.2.2).
- Minimum number of crack growth increments for stabilized crack closure values – the crack needs to propagate a certain distance in the numerical model to obtain steady state behavior (section 3.2.3). Steady state behavior means, in this case, that the calculated crack closure level has stabilized when propagating the crack further (see Figure 3.10).
- The definition of closure. Different definitions have been used by recent researchers and it is clear that they will give different values [13] (section 3.2.4).

This numerical analysis aims to find closure levels using the same geometry and inputs as in the experiments already conducted by VAC at their test lab in Trollhättan. The 3D-geometry is shown in Figure 3.1 and the actual material modeled is cast Inconel 718.

3.1 Model

The model of the Kb-specimen considered in this thesis is depicted in Figure 3.1 (a). It consists of a semi-circular surface crack with an initial size, $a_i = c_i = 2$ mm with thickness, $t = 4.27$ mm, width, $W = 10.16$ mm and height, $H = 31.76$ mm. The model is subjected to mode I loading, which makes it possible to utilize two-fold symmetry allowing modeling of only one-quarter of the specimen, as shown in Figure 3.1 (b). One symmetry plane is along the crack surface and the other is the center plane parallel to loading direction extending in the direction of the thickness.

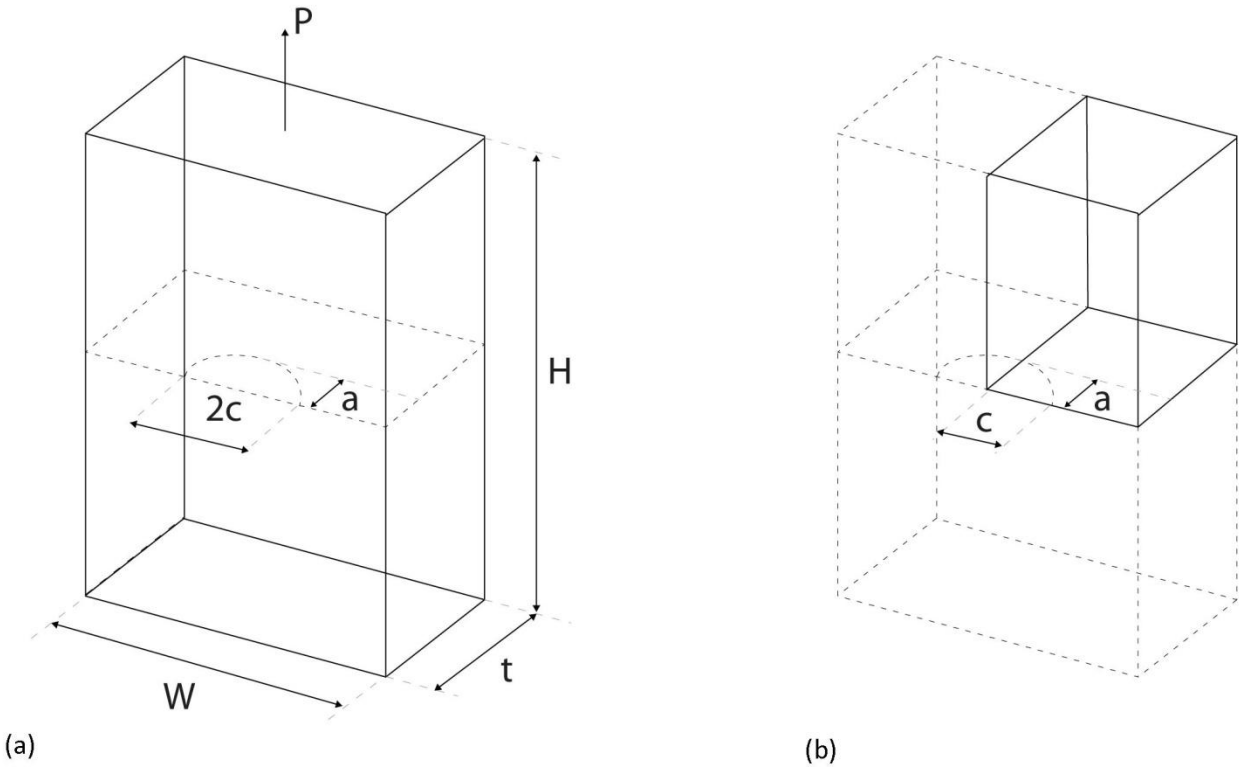

Figure 3.1: (a) Model of the Kb-specimen and (b) model of the Kb-specimen utilizing two-fold symmetry.

The crack is assumed to be semi-circular, i.e. $a = c$, at all times, and thus only one single parameter will be used to describe the current crack length. This assumption originates from the experimental results which indeed shows that the crack often grow in a semi-circular manner (see Figure 3.7).

3.1.1 Mesh

The model is built up by 8-node structural solid elements (SOLID185 in ANSYS [14]) with each node having three degrees of freedom; translations in the nodal *x*, *y* and *z* directions. A typical mesh is shown in Figure 3.2. Ahead of the crack tip a fine mesh with rectangular elements of equal size in radial direction is used, shown in Figure 3.2 (c). This allows simultaneous and equidistant propagation of the crack along the crack front. A typical mesh consists of 55 000 nodes and 70 000 elements.

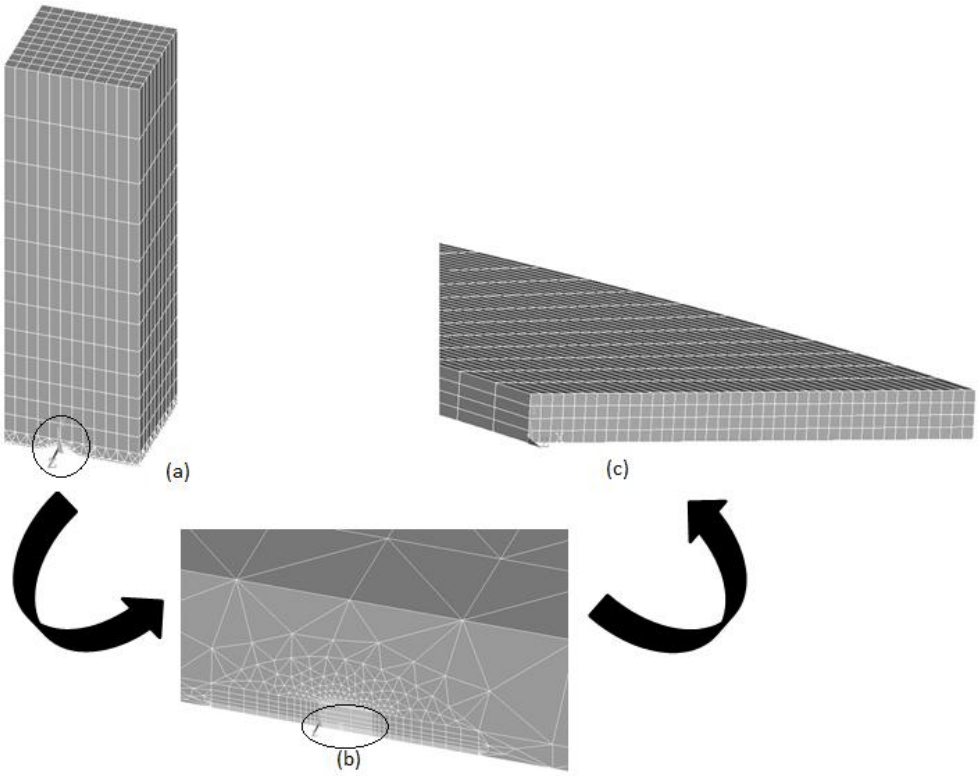

Figure 3.2: Typical finite element mesh (scaled): (a) Overall view (b) transition from near crack tip domain to outer domain (c) close up view at crack front in propagation direction.

In the circumferential direction (φ-direction in Figure C.2) a somewhat large element aspect ratio of approximately 20 has been used, this is applicable since ΔK is close to constant in the circumferential direction due to a balanced geometry (see Appendix C for a comment on this reasoning).

It is important to keep down the number of elements as well as having a smooth transition from the fine mesh at the crack tip to the coarse mesh. A linear hexahedral element type is used at and around the crack tip according to the black element in Figure 3.3 (a). A transitional mesh consisting of 4-noded linear tetrahedral elements has been used according to the red element in Figure 3.3 (a), regardless of the violation of the C^0 continuity. Using 4-noded linear tetrahedron will significantly reduce the degrees of freedom leading to that this meshing issue is a trade-off between loss of accuracy and computational effort. A test of which method is the most accurate has been performed and it is clear that using quadratic elements has a very marginal effect of the closure levels (see Appendix C).

Figure 3.3: Elements in the transitional mesh, (a) non-matching mesh between hexahedral and tetrahedral elements at the common surface thus violating C^0 continuity, (b) consistent transition between hexahedral and pyramidal elements that is recommended by ANSYS for this kind of transitional mesh.

3.1.2 Boundary Conditions

The model is subjected to mode I loading. Symmetry conditions are imposed at the symmetry boundaries according to Figure 3.1 (b). Frictionless contact conditions at the bottom symmetry plane, are imposed with a rigid target area. Loading of the model occurs through an applied pressure load at the top boundary. To accurately confine crack growth and contact leading to closure and opening behavior, the load steps for every cycle need careful designs. It should be refined in areas where the closure and opening levels are expected to be found since the finite sized load step will resolve the opening level to the same magnitude as the load increment. See Figure 3.4 (a), (b) and (c) for further explanation. The figures below illustrate variably sized increments of one load cycle for different *R*-ratios. Preliminary studies pointed out a requirement of 40 increments for $R = 0$ and $R = 0.5$ and 65 increments for $R = -1$. Additional substeps are implemented near zero load where contact nonlinearities require smaller increments.

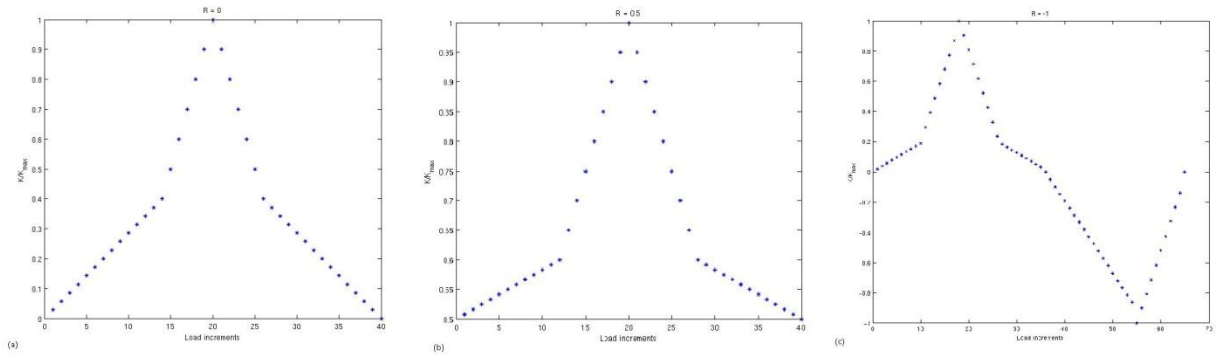

Figure 3.4: Details of load cycles of (a) $R = 0$, (b) $R = 0.5$ and (c) $R = -1$. Variable sized increments will provide better resolution.

3.1.3 Material

Cyclic plastic deformation of the material near the crack tip is difficult to model, since effects such as strain ratcheting, stress relaxation and cyclic hardening or softening are often apparent. Most common engineering materials exhibit a linear stress-strain relationship up to a stress level known as the proportional limit. Beyond this limit, the stress-strain relationship becomes nonlinear. This analysis uses a multi-linear kinematic hardening constitutive model that can incorporate the Bauschinger effect to describe the cyclic elastic-plastic response of the material. The particular method of choice is the Besseling model [14], also called the sublayer or overlay model, which has different yield stresses for each subvolume that is specified by the same Young's modulus. The backstress uses a stepwise linear relation to plastic strain as in Figure 3.5. The material data used in this work is produced by VAC for cast Inconel 718.

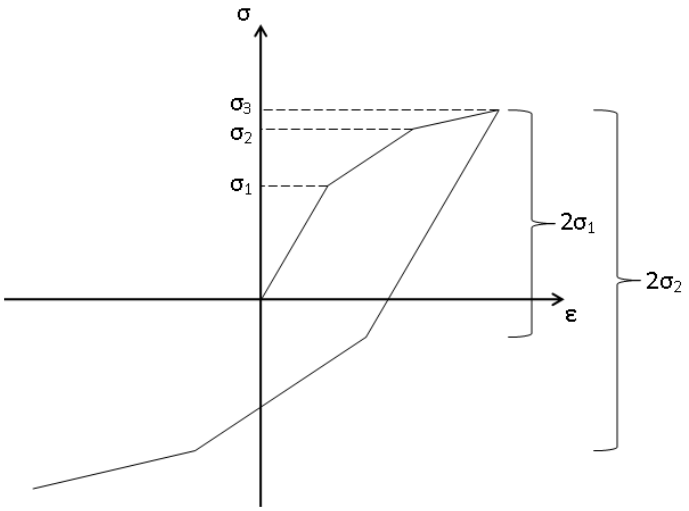

Figure 3.5: Loading and unloading behavior for a multi-linear kinematic material model in ANSYS.

3.1.4 Mesh requirements for convergence

At the crack tip the stress magnitude is highly intensified and therefore small elements must be placed both near the crack tip and along the direction of crack propagation. The size of the forward- and the reversed plastic zones are main parameters to consider and there are many papers on mesh criteria for 2D FE-analysis of fatigue crack growth. However, many researchers have neglected this issue for their 3D models, which might be due to the computational effort needed. Especially the effect and requirement of using finite size geometry are lacking investigation. Skinner and Daniewicz [16] did investigate closure in a finite rectangular plate with a semielliptical surface flaw subjected to remote tension loading. They concluded that five elements in the forward plastic zone at the deepest point of penetration are sufficient for mesh independent closure loads. However, they used a simple constitutive material model that omits the Bauschinger effects which results in that their conclusions are difficult to interpret to the current analysis. Roychowdhury and Dodds [12] found in their small scale yielding analysis that 10 elements in the forward plastic zone in fact could give an adequate solution. The mesh also needs to have sufficiently small elements to capture reversed yielding at the crack tip upon unloading [17]. Roychowdhury and Dodds [12] suggest that 2-3 elements should be fully contained within the reversed plastic zone at the end of the first cycle. They made a detailed study on mesh convergence and suggest that the mesh needs to satisfy three conditions: (a) the plastic zone on the crack plane at peak load encloses more than 10 eight-noded brick elements, (b) the reverse plastic zone at zero load encloses at least two elements, and (c) the half-thickness has at least five elements layers.

For the analysis a multi-linear material model is used and the forward plastic zone size is defined as the number of elements in the crack plane experiencing equivalent plastic strain magnitudes above 0.002 at the first peak load. The definition for the reversed plastic zone is the number of elements experiencing a change of 0.002 equivalent plastic strain between the first peak and minimum load. It is sufficient to investigate this at the first cycles since these values will remain almost unchanged at later cycles [18]. The mesh seems satisfactory when 2 or more elements are contained in the reversed plastic zone and 5-

10 elements in the forward plastic zone. In this case, this means that for R = 0 the element length (L_e) needs to be 0.005 mm and for R = 0.5 and R=-1 L_e must be equal to 0.0025 mm or smaller. The increased mesh refinement needed for R = 0.5 is a result of a smaller crack tip reversed plastic zone as discussed in ref. [19]. The reason for the tougher mesh requirement for R = -1 is due a lower maximum applied load yielding a smaller plastic zone.

In addition to the requirements on the element size in the radial direction, it is also imperative to have sufficient number of elements in the circumferential direction. This is especially important near the free surface, where the results have shown to have a higher variation of the opening levels, which can be anticipated by inspecting Figure 3.6. The figure shows the plastic zone at the free surface at peak load and the greatest variation of the size can be seen near the free surface.

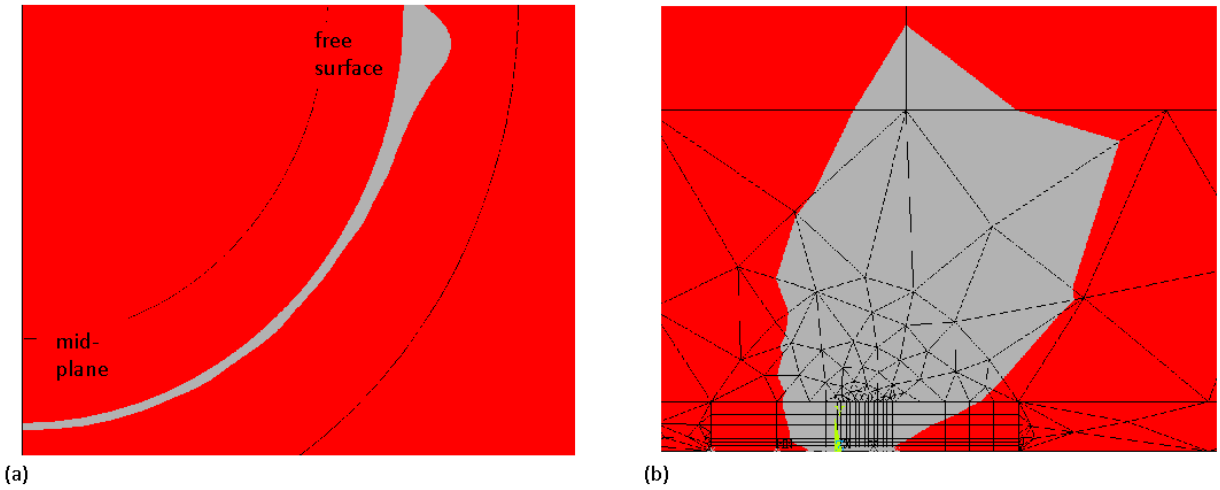

Figure 3.6: Forward plastic zone (a) along the crack front indicating larger forward plastic zone near the free surface and (b) at the free surface.

3.1.5 Computational code

The global solution is obtained by a built in Newton-Raphson algorithm in ANSYS. On an average 4-6 iterations are needed to reach equilibrium for residual forces and to satisfy contact condition at each load increment. Each load cycles requires between 40 – 65 load increments, depending on the R-ratio , with additional substeps close to zero load and unloading for R = -1. The crack extends one element in each of 20-40 load cycles in order to grow the crack into a steady state condition. A typical analysis takes about 1 minute per iteration leading to a wall-clock time varying between 3-7 days on a Dell Precision T7500 machine with 2 Intel® Xeon® X5660 processors.

3.2 Crack propagation scheme

3.2.1 Crack tip node release

The crack propagation in the numerical analysis should ideally reflect the experimental results. It is observed in the experiments that the crack grows in a semi-circular manner (Figure 3.7). Thus, in the FE-simulations it is assumed that the crack propagates keeping its semi-circular shape during propagation. Due to the complexity of modeling the shape evolution, the shape effect is neglected and the crack tip growth is modeled by advancing the crack through the thickness of the geometry. The crack propagates uniformly over the crack front by an increment of one element (Δa) in each cycle after releasing all the nodes at the crack front after the last unloading step. This method does not truly represent a real

fatigue process since a crack is not expected to propagate in a compressive stress field and the crack front is not expected to propagate in all directions simultaneously. This procedure is implemented to overcome convergence issues that often appear by propagating the crack at maximum load. Several studies have shown that releasing nodes at different stages during the load cycles has an insignificant effect on the results [3, 20] and this test is therefore omitted in the analysis.

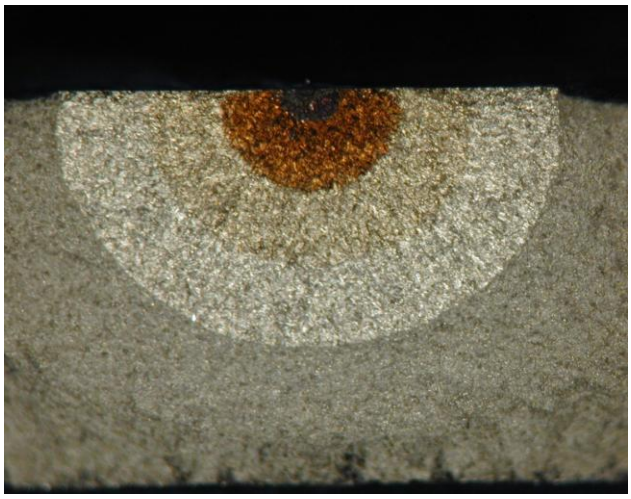

Figure 3.7: Example of the fracture surface of a Kb-specimen.

3.2.2 Load cycles per node release

The analysis uses a 1-node-per-1-cycle debonding scheme, resulting in a growth of 2.5, µm/cycle ($da = L_e$), which is significantly higher than actual da/dN. According to VAC's experiments of cast Inconel 718 a typical crack growth for $R = 0$ is of a magnitude of 0.04 µm/cycle, for $R = 0.5$ it is 0.02 µm/cycle and for $R = -1$ it is 0.1 µm/cycle for measured ΔK. To mimic the experiments one would either need to increase the number of load cycles per node release or to reduce the mesh size. Both approaches would lead to impractically long computational times.

Rodriguez and Antunes [13] discuss the importance of using several load cycles per node release in order to stabilize the cyclic plastic deformation to achieve reliable results. Apparently 2-cycles-per-node release should be enough depending on material model used in the analysis. Matos and Nowell [21] conclude that up to 8 cycles between node releases could be necessary in a 3D analysis. Such a large number of cycles per node release will drastically increase the computational effort and rule out an analysis such as this one. Borrego, Antunes, Costa and Ferreira [10] claim that the number of cycles between node release depend on when the nodes are released in the cycles. If the nodes are released at peak load, the deformation near the crack tip causes a too large closure stress. If that scheme is applied, two or more cycles are needed before measuring the closure level. This effect has faded out during unloading and therefore by using a node release scheme at the last unloading step only 1 cycle is necessary.

From Figure 3.8 (a) and (b) it is evident that using 2-cycles-per-node release will indeed give different results compared to 1-cycle-per-node release for $R = 0$. Along the crack front the closure level is shifted between 3 – 9% vertically but the shape throughout the crack front is identical. This difference is

considered to be of acceptable level. In addition, adding one cycle would more than double the analysis time, which is not feasible. No test of 3 or more cycles-per-node release has been made. Future analysis should consider a 1-node-per-2 cycle scheme in order to capture closure level accurately.

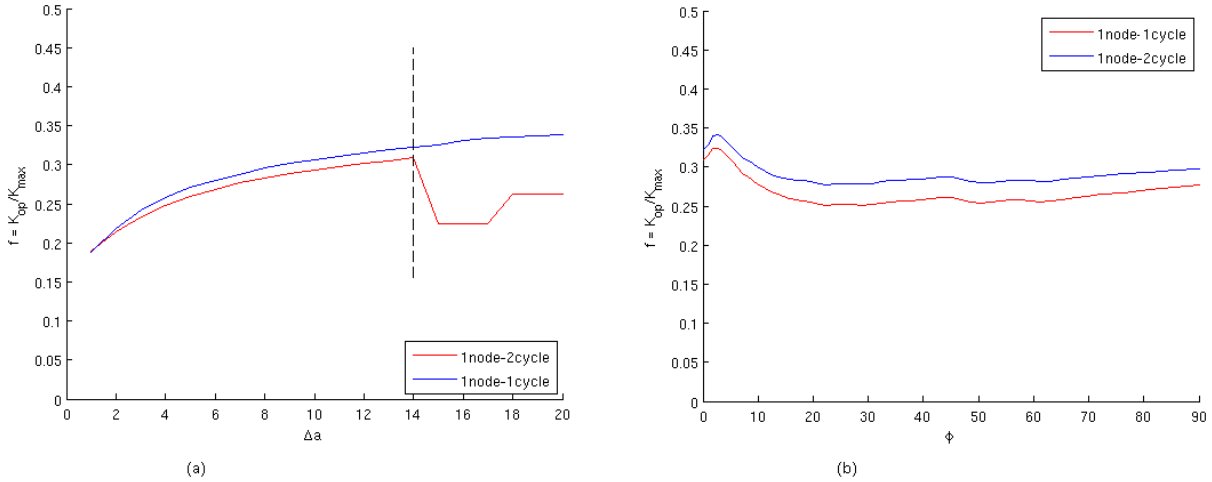

Figure 3.8: Comparison of closure level for different number of load cycles per node release. (a) at $\phi = 90^0$ and (b) along the crack front after 14 node released. The dotted line in (a) signifies onset of an unexpected numerical error in the analysis. These analyses correspond to: R = 0, L_e = 0.005 mm, T = 20 ^oC.

An unexpected feature is noticeable in the same figure; after 14 released nodes are a sudden drop in closure level for the 1-node-per-2-cycle scheme. This numerical error is most likely due to that a too loose convergence criterion was used in the global Newton-Raphson algorithm. Rodriguez [13] point out that this can happen when large deformations exists in the analysis together with other nonlinearities such as contact conditions. Due to the time constraint of this thesis further investigations of this error were not conducted.

3.2.3 Crack growth for stabilization

It is desired to have a suitable criterion for minimum crack extension required in order to obtain steady state values for crack closure and opening. Earlier studies suggest the initial forward plastic zone as a measure and indicate that to achieve convergence the crack should propagate all through the initially deformed material [10,12-13, 16, 22]. The reasoning is that a material point right behind the crack tip needs to accumulate all plastic strain from a complete deformation history, see Figure 3.9 for clarity. A point located inside the initial forward plastic zone does not accumulate enough plastic strain by the time the crack has propagated through it. Many authors show different results regarding how far the crack should propagate in relation to the initial plastic zone. It has been recommended that a convergence study for every specific analysis should always be performed. The ratio of crack propagation over the size of the forward plastic zone ($\Delta a/r_p$) is used as a measure in this analysis.

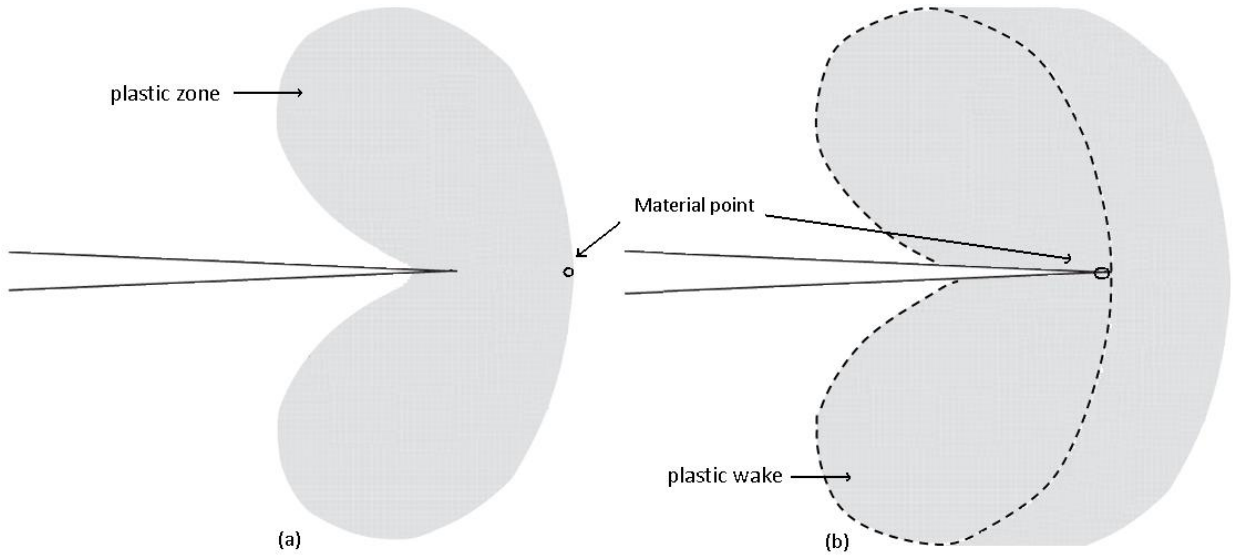

Figure 3.9: Plastic zone of (a) before cyclic loading and (b) after a propagating the crack a complete loading history. Note the location of one material point.

The curve in Figure 3.10 demonstrate the development of $f = \frac{K_{\mathrm{op}}}{K_{\mathrm{max}}}$ obtained for R = 0 at mid plane ($\phi = 90^0$) by propagating the crack from the initial crack size by increments of one element (Δa). The normalized opening value, f, first increases and then stabilizes as the effect of the initial plastic wake is disappearing. Since the crack is only allowed to grow a relatively short distance (compared to other characteristic dimensions), the longer crack at the end of the growth does not significantly influence the stress intensity factor. After about 10 increments (10 Δa) the crack closure has stabilized and a steady state value can be found. Consider the larger plastic zone at the free surface, where the stress gradient is higher, it is seems obvious that more nodes need to be released to achieve stabilized values there.

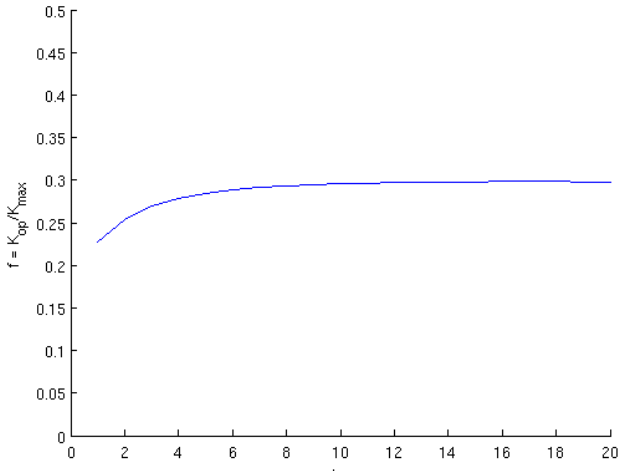

Figure 3.10: Closure level as a function of increments, R = 0, L_e = 0.005 mm, T = 20 ^{o}C.

This is also apparent when examining plots similar to Figure 3.10 for those degrees. It would, although, cause a huge computational effort if stabilized values were strictly to be found around the entire circumference, however, since the final opening level determined is calculated as a weighted average of all the opening levels at all degrees at the crack front, it has a minor effect of not fully capturing the opening level at only a few degrees. Rodriguez [13] proposed an interesting extrapolation method for this issue which is described in Appendix D.

A convergence study for this numerical analysis was established defining yielding where $\varepsilon_p = 0.002$. With this definition of yielding, the forward plastic zone is calculated at peak load and it seems to be sufficient to let the crack propagate 1-2 times this distance for R = 0, see Table 3.1 for more details. The great variation of $\Delta a/r_p$ implies that careful consideration should be taken if this measure is to be used as a criterion. It can be concluded that the ratio is related to the R-ratio. It can also be concluded that closure levels converge slower at R = 0 and R = -1, where the reversed plastic zone is considerably smaller.

Table 3.1: $\Delta a/r_p$ for different temperatures, R-ratios and degrees at crack front.

R = 0	**T = 20 °C**	**T = 650 °C**
ϕ = 0°	>1.8	>1.2
ϕ = 45°	1.2	1.6
ϕ = 90°	2.0	2.5
R = 0.5		
ϕ = 0°	>0.5	>0.45
ϕ = 45°	0.1	0.2
ϕ = 90°	0.3	0.3
R = -1		
ϕ = 0°	>1.1	>1.6
ϕ = 45°	2.5	3.1
ϕ = 90°	3.1	5.0

3.2.4 Closure definition

There are many definitions that could be considered when defining crack closure. It is a key issue in a numerical aspect, because of the large variation of closure results. Most 3D and 2D studies determines opening levels by monitoring the displacement or the reaction force of each node on the crack surface, or the stress of each element adjacent to the crack surface behind the crack tip [23]. The present analysis defines the opening level, K_{op}, according to [22], i.e. defining opening when the first node behind the present crack tip loses contact to the symmetry plane. When this occurs the crack will be fully opened and no point at the crack surface will remain in contact. Likewise, the closure level, K_{cl}, is defined when the first node behind the present crack tip first come into contact with the symmetry plane during unloading. Rodrigues and Antunes [13] conclude that closure levels will increase if nodes closer to the crack tip are chosen to define closure. In other words, using for example the second node behind the crack tip will decrease the closure level as is evident by studying Figure 3.11. It also means that using smaller elements at the crack tip would increase the closer level. They explain this effect by the occurrence of plastic deformation at the crack tip at the same time that the nodes closest to the crack tip open. Wu and Ellyin [24] conclude in their 2D study that the above described method is not accurate enough. They propose that the nodal reaction force at the crack tip should be monitored and

when it becomes tensile the crack has a potential to propagate, and thus the crack is open. Likewise for closure, when the reaction force becomes compressive at the crack tip, the crack no longer has a potential to propagate and hence, the crack is considered as closed. Most researchers, as well as the current analysis, defines closure based on the first node behind the crack tip [10, 18], however for further analysis careful consideration should be taken when choosing. The results from a numerically analysis should ideally be compared to some measured crack closure data as a foundation for finding best matching definition.

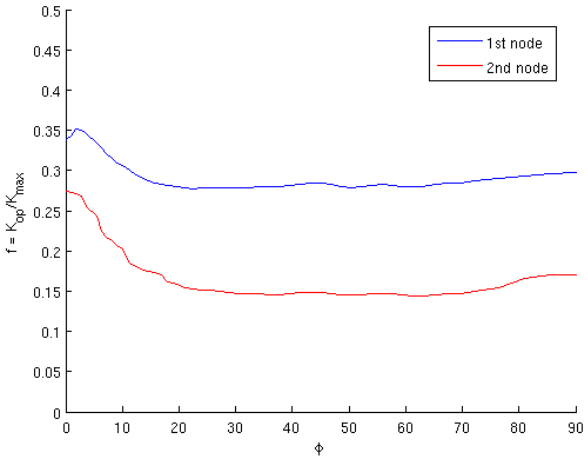

Figure 3.11: R = 0, L_e = 0.005 mm, T = 20 °C. Difference of opening defined by first node behind the crack tip and second node behind the crack tip. The different definition give a discrepancy of more than 40 % comparing the weighted average of f.

Crack closure and opening levels are normally regarded to differ slightly; closure level is consistently lower than the opening level. This difference is often neglected since it is usually considered small. This difference increases when the maximum stresses increases [17]. Opening is commonly regarded to be more important in a physical sense to the crack propagation mechanism, hence more often used in the analytical calculations. This FE-simulation shows that for the case studied closure levels are significantly lower than opening (see Figure 3.12). The reason for this large difference is thought to be that relatively high maximum stresses over flow stress are applied. It could also be due to effects of the finite size geometry or that the mesh at the crack front is unable of resolving enough of the reversed plastic zone.

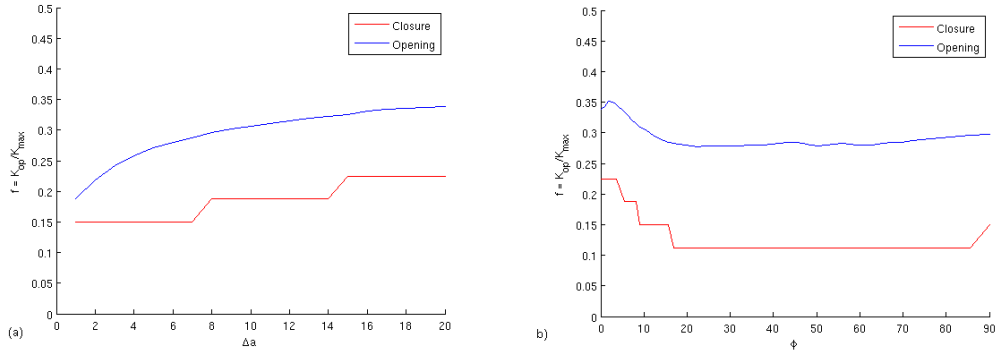

Figure 3.12: R = 0, L_e = 0.005 mm, T = 20 °C. Comparison of opening and closure levels, (a) $\phi = 90^0$ and (b) along the crack front. The numerical analysis resolves closure by magnitude of one load increment.

3.3 Convergence study

Two criteria to check when analyzing crack closure results are: 1. has the crack propagated into a steady state region? 2. Does the employed mesh sufficiently fine? In general, the first question has to be checked upon for every run, however question two is sufficient to investigate only once. Figure 3.13 compares $f(\phi)$ curves when releasing 40 and 20 nodes (during 40 and 20 load cycles), respectively, for R = 0 and T = 20 °C. At the free surface the opening levels are amplified and in this region the largest difference is approximately 0.035. As was illustrated in Figure 3.15 (a) and (b) the opening level is not fully stabilized at 20 nodes released for small ϕ, which indicates that more crack growth is necessary to obtain steady state values. Nonetheless, the difference is negligible and it is concluded that a sufficient number of nodes are released. In addition the weighted average of f along the crack front will reduce this discrepancy even more. The contribution from the closure levels at the free surface appears marginal on the weighted average of f.

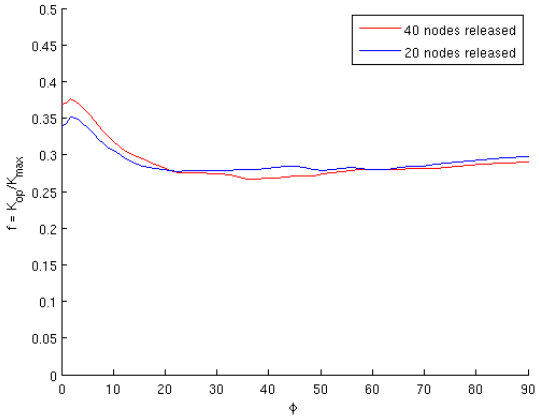

Figure 3.13: Comparison of 40 node released and 20 node released of stabilized opening levels as a function of ϕ for R = 0 and T = 20 °C.

The verification of the mesh has previously been discussed in context of the forward and the reversed plastic zone. The number of elements in the forward and reversed plastic zone can be found in Table 3.2.

Table 3.2: Elements in forward and reversed plastic zone (T = 20 °C, $L_e = 0.0025$ mm).

	ϕ = 0°		**ϕ = 45°**		**ϕ = 90°**	
T = 20 °C	Frw. Pz	Rev. Pz	Frw. Pz	Rev. Pz	Frw. Pz.	Rev. Pz.
R = 0	40	17	21	5	13	4
R = 0.5	>49	4	36	1	18	1
R = -1	29	24	13	10	9	8
T = 650 °C						
R = 0	29	13	13	3	9	3
R = 0.5	>49	4	31	1	16	1
R = -1	25	20	10	8	7	6

To show that a mesh of $L_e = 0.005$ mm produces converged results, the opening levels are compared with a mesh of $L_e = 0.0025$ mm for $R = 0.5$ at T = 20 °C. The case $R = 0.5$ is chosen since this ratio has tougher requirements on the size of forward and reversed plastic zones. The two different meshes have the same general set-up, although with different element sizes near the crack tip area. Note that 40 nodes are released for the mesh using $L_e = 0.0025$ mm, thus the cracks are grown equally far. From Figure 3.14 it can be concluded that the mesh indeed satisfy convergence criteria.

3.4 Results

This numerical analysis establishes opening levels for a set of load conditions that corresponds to the experimental tests performed at VAC. The main objective is to obtain the opening levels, *f*, for a variety of temperatures and *R*-ratios. Finally, to make use of NASGRO® (see NASGRO manual [9]) the opening values have to be connected to determine an unequivocal value of the parameter α.

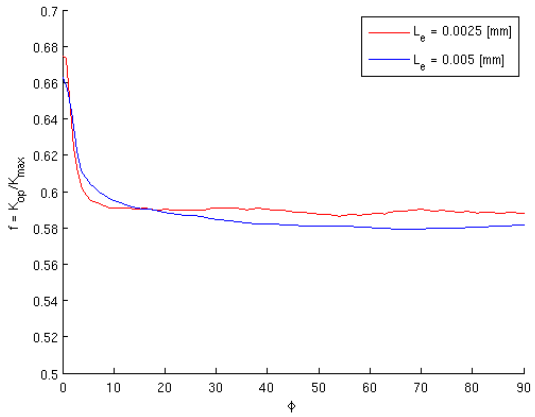

Figure 3.14: Stabilized opening levels as a function of ϕ for $L_e = 0.0025$ mm (red) and $L_e = 0.005$ mm (blue).

The opening levels have been obtained for two different temperatures, T = 20 °C and 650 °C, and for three different *R*-ratios, $R = 0, 0.5$ and -1. Table 3.3 shows applied loads for respective temperature and *R*-ratio.

Table 3.3: Applied loads used in the numerical analysis for respective temperature and *R*-ratio. Only mode I membrane loading is applied throughout the analysis.

	T = 20 °C		T = 650 °C	
R - ratio	Max stress [Mpa]	Min stress [Mpa]	Max stress [Mpa]	Min stress [Mpa]
0	555	0	400	0
0.5	605	302.5	475	237.5
-1	500	-500	375	-375

Two different meshes have been used in order to contain sufficient number of elements both in the forward and reversed plastic zone; one with element size, $L_e = 0.005$ mm and one with $L_e = 0.0025$ mm. The definition of the forward plastic zone size is the number of elements in the crack plane experiencing equivalent plastic strain above 0.002 at the first peak load. The definition for the reversed

plastic zone is the number of elements experience a change of 0.002 equivalent plastic strain between the first peak and minimum load. The number of elements in the forward and reversed plastic zone can be found in Table 3.4 for T = 20°C, $L_e = 0.005$ mm, all *R*-ratios and at three locations at the crack front. These results are helpful when determining the accuracy of the model and to get an idea of how far the crack should propagate to achieve steady state behavior. Table 3.1 shows a summary of the ratio $\Delta a/r_p$ (distance of crack propagation over size of forward plastic zone).

The combination *R* = 0 and T = 20 °C has been used as a template to obtain reliable results. It is assumed that the mesh with $L_e = 0.005$ mm is sufficiently fine to capture the opening behavior for this case, since it satisfies recommendations from several researchers [12-13, 17] and provides reliable results.

Table 3.4: Number of elements contained in forward and reversed plastic zone for T = 20 °C, $L_e = 0.005$ mm.

T = 20 ?						
Le = 0.005	Θ = 0°		Θ = 45°		Θ = 90°	
	Frw. Pz	Rev. Pz	Frw. Pz	Rev. Pz	Frw. Pz.	Rev. Pz.
R = 0	22	9	10	2	7	2
R = 0.5	31	2	18	1	11	0
R = -1	16	14	6	3	4	3

Figure 3.15 (a), (b) , (c) and (d) shows the opening levels for $R = 0$, T = 20 °C at $\phi = 0^o$ (free surface), 5.4^o, 45^o and 90^o (mid-plane), respectively, with 20 nodes released. The chosen number of released nodes is based on the elements in the forward plastic zones. For $\phi = 45^o$ and $\phi = 90^o$ the crack has propagated into the steady state region and stabilized values are found at around 10 increments, which corresponds to the number of elements in the forward plastic zone. This agrees well with theory of crack growth for stabilization described in section 3.2.3. At $\phi = 0^o$, the steady state region has not yet been reached and a strict stabilized value cannot be confirmed, as expected by examining the size of the forward plastic zone. In this region the plastic zone is significantly larger and the crack has not grown far enough for stabilization to occur.

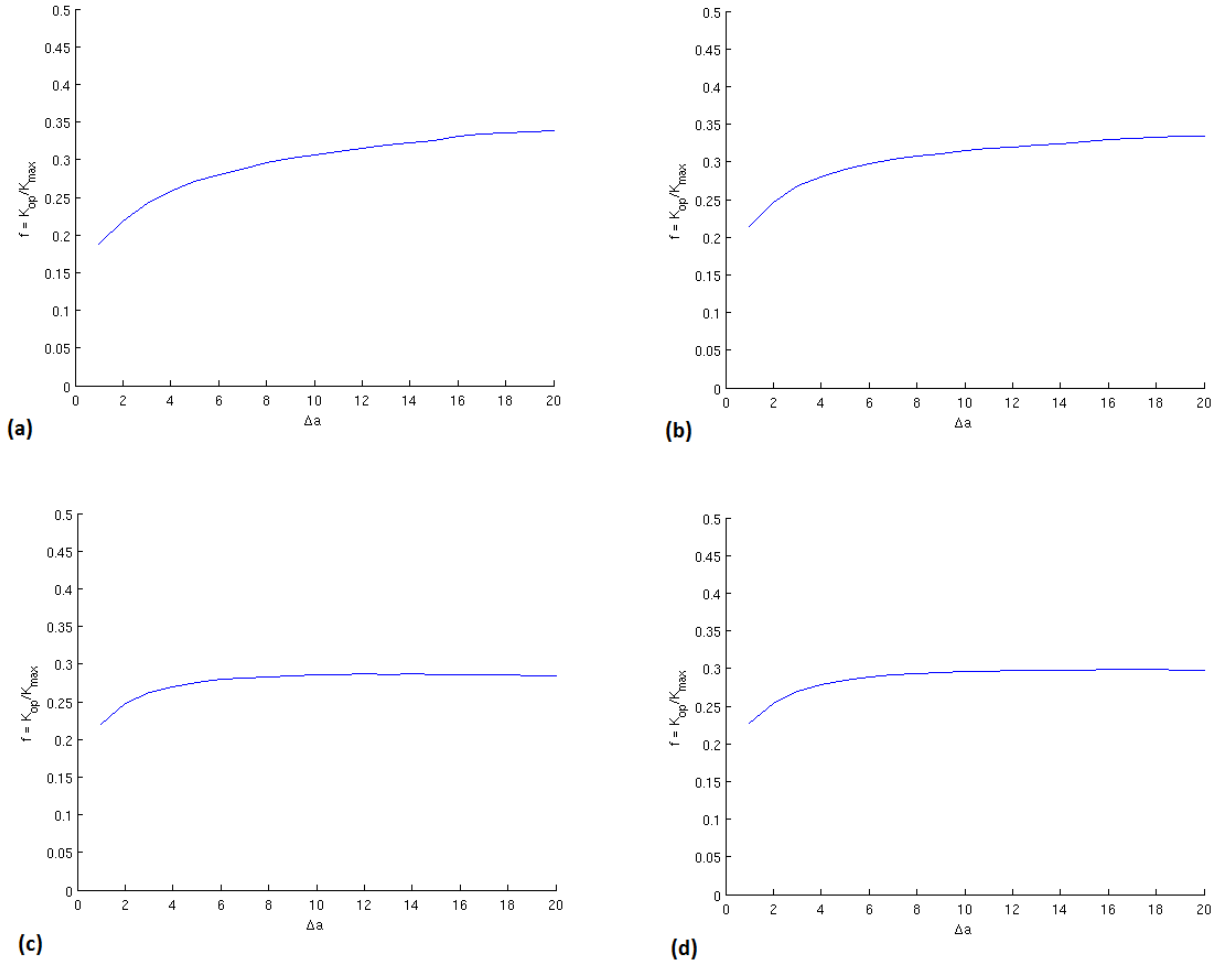

Figure 3.15: Opening level for *R* = 0, T = 20 °C and 20 node released at (a) $\phi = 0^o$(free surface), (b) $\phi = 5.4^o$, (c) $\phi = 45^o$and (d) $\phi = 90^0$(mid-plane).

Hou [15] concludes that the plastic wake for a semi-circular crack can be separated in two categories: (1) wake near the surface, and (2) wake in the interior region. For visualization, study Figure 3.6 which shows the forward plastic zone as a function of ϕ. The near-surface wake is caused by the surface plane stress and is larger than towards the interior region. This indicates opening occurs later since the shape of the contact region of the crack surface is similar to the shape of plastic wake. Figure 3.16 depicts opening level across the crack front from the free surface to mid plane (i.e. (ϕ)) and the variation of f is accordingly to Hou's conclusions. The opening level is larger towards the free surface following the appearance of the plastic wake. Outside this region, which extends typically to 8-10°, the opening level is quite constant. In order to establish an estimate of the NASGRO® parameter α for the load condition and temperature a single value of f, based on the variation along the crack front, is necessary. A single value of $f(\phi)$ is determined by a weighted average and, as described in Section 2, α can then found by solving the set of nonlinear equations (2.8) – (2.12).

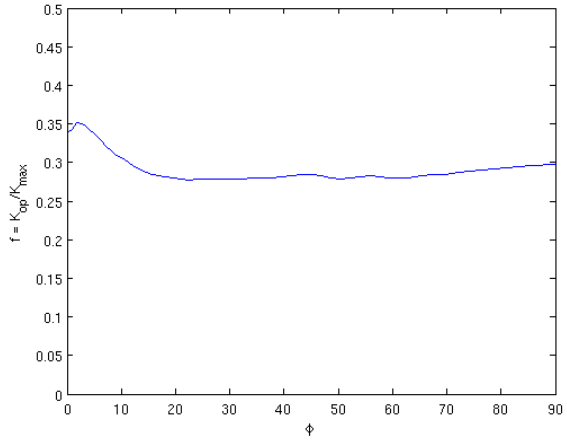

Figure 3.16: Stabilized opening levels, *f*, as a function of ϕ for *R* = 0, T = 20 °C and 20 node released.

Table 3.5 below summarizes the results from the different cases, for plots of the closure behavior see Appendix A. The value of $\sigma_{\max}/\sigma_0$ and the corresponding value of α is also included. It can be seen that the value of f does not change considerably for the two different temperatures. Even if the material properties are changed with increasing temperature, the applied loads have been changed accordingly in the experimental testing. This results in a fairly constant $\frac{\sigma_{\max}}{\sigma_0}$, thus constant values of f are expected. Values of α varies from 1 to 3 leading to that determining an unequivocal value is not straightforward. The variation of α is discussed in chapter 3.5.1. Simply, an average of these values is chosen as the best method.

Table 3.5: *f* and α different temperatures, *R*-ratios and degrees at crack front.

Temperature (°C)	R	f	σ_{max}/σ_0	α	Mesh
20	0	0.29	0.52	1.95	*Le*05
20	0.5	0.59	0.56	1*	*Le*025
20	-1	0.09	0.47	3*	*Le*025
650	0	0.31	0.45	1.93	*Le*05
650	0.5	0.59	0.54	1*	*Le*025
650	-1	0.13	0.42	3*	*Le*025

*An α could not be found within the range of Newman's crack opening function and the closest value is used. See Figure 2.5 for clarification.

3.5 Discussion

Comprehensive numerical calculations for 3D crack closure levels lead to a large demand of computer capacity. This includes problems of both disc space and wall clock time. With these aspects in mind, the model and the calculation schemes in use need to reflect what realistically can be done within a project, but they also have to reflect the real life situation of fatigue crack growth. The model for crack closure should, most importantly, consist of sufficient small elements at the crack front in order to capture the high stress gradients and deformations. This means that an adequate number of elements must be contained within the forward and reversed plastic zones. However, there will always be certain

shortcomings in the model to avoid too large computational demands. These may or may not affect the results. One has to validate the model.

The shortages that may exist in the model have been investigated and adequate decisions have been made to obtain a valid solution whilst keeping down the computational time. The main uncertainties, regarding the model, was the element size at crack tip area, the aspect ratio of the elements, the element ratio between the fine and the coarse mesh and the non-matching mesh within the transition part. Verification of the employed solutions have been performed, although separately and independent from each other. What would be desirable for further validation of the numerical model is to compare the predicted closure levels with a refined model without the shortcomings described. Will this make a notable impact of the results even though they each independently don not?

Other fundamental aspects for producing reliable results are node release schemes; number of load cycles between node releases, where in the cycle crack tip node release happens, closure definitions, required crack growth for stabilization of the closure levels etcetera. It was concluded that the numbers of load cycles between node release makes a difference of about 7 % on the weighted average of f. It is also evident that the difference of closure and opening levels are large as well as that closure definition is a key issue. Some parts of the crack front do not reach a steady state response and it is not always possible to produce such stabilized values. This has, as discussed in section 3.3, had negligible effect on the results. However, the extrapolation method described in Appendix D is recommended for further use if lack of time will put limits on longer crack propagation.

The material model will also significantly affect the magnitude of closure. Using an isotropic hardening material model has shown, in a preliminary study, to give notably larger values. There are other options not evaluated such as the Ellyin–Xia model, proposed by Ellyin and Ozah [23]. This model predicts a lower crack opening stress profile compared to a kinematic hardening. The model captures the unloading and reloading path accurately by employing two hyper-surfaces and two types of loading regimes. It produces, according to the authors, opening stress values with good agreement to experimental results.

One can easily conclude that the uncertainties in numerically calculated closure levels are many. With the lack of experimental testing (and knowledge of how this should best be performed) to verify the results of closure it is a difficult task to be confident on the accuracy of the results. It has been showed that numerically calculated opening values in general are higher than experimentally measured [16]. Little is known about the uncertainty of the experimental measurements and numerical analysis leading to difficulties of drawing general conclusions. However, since recommendations of current research are followed and proper investigations have been performed of known error sources the results should be considered reliable.

A further uncertainty is the assumption of the crack shape during growth. The crack propagation process can be seen as a stochastic process and the shape of the crack will not always remain semi-circular. There is plenty of experimental evidence that the shape of a 3D crack front in fact changes as the crack grows during cyclic loading [24, 25]. Although, it is a questionable assumption in that context, the purpose of this numerical study is to establish the closure level and its 3D variation along the crack front and for that reason the growth process itself might not be important. The importance lies in the crack geometry when it has reached the steady state region. The shape of the crack is important in other

contexts since this, along with crack closure and stress state, may influence further development of the crack shape when growth occur. Many studies have been devoted to this problem with Newman and Raju as pioneers [26]. As of the authors' knowledge, few have performed numerical 3D investigations of crack growth taking account of closure effects; however, this issue is outside the scope of the thesis but could be an important future step. In the NASGRO® software a crack closure factor is multiplied with ΔK to produce more accurate crack growth predictions, which is applied where the crack front intersects a free surface [9].

One problem that has occurred at a few simulations is a sudden drop in closure; studying Figure 3.8 one can draw conclusions of apparent errors. It is most likely of numerical characteristic, regarding a too large value for the global convergence tolerance. Current nonlinearities, such as large deformation and contacts during opening/closure, needs to be taken into account when deciding on method and tolerance for finding a global solution. Further investigation of this parameters effect on the results is desired.

3.5.1 Plane stress/strain constraint factor, α

The main purpose for this numerical analysis was to produce an unequivocal value of the parameter α. This parameter is described by Newman [8] as a geometrical parameter regarding the stress state in the specimen. As can be understood by the previous sections a single value could not be found for different *R*-ratios. No investigations are conducted to find out if it is the shortcoming of the theoretical model used to establish such a value or there are other reasons.

Though the variation of the opening function, f, has been concluded along the crack front there are still difficulties to obtain how the stress/strain parameter, α, varies. This is due to two reasons:

1) α is highly dependent on the value of $\frac{\sigma_{\max}}{\sigma_0}$
2) different values of α are obtained depending on the R-ratio.

The problem with the first point is how to define the flow stress, σ_0, which is the instantaneous value of stress required to continue deforming the material. For convenience it is often set to the average of the yielding and ultimate strengths, which will result in a loss of accuracy per se. It is still a problem of how to define the yielding and ultimate strengths for a material experiencing non-linear, plastic behavior.

The second point causes an even larger problem when obtaining α. Since α is a geometrical constant it should not be dependent on the stress ratio. However, from the values of f obtained from the numerical analysis it is not possible to get a unequivocal value of α, and it is only for $R = 0$, where a solution could be found. For $R = 0.5$ and $R = -1$ the value have been chosen as 1 and 3, respectively since these where the closest values to a solution, seen in Appendix B for the specific choice of $\frac{\sigma_{\max}}{\sigma_0}$. It is obvious that the expected relationship between f and α based on Newman's crack opening function (2.8), has not been captured with the results from the numerical analysis. One of the reasons that a unique relation was not obtained might be to the fact that the specimen considered does not fully fulfill the LEFM conditions as discussed in section 3.5.2.

3.5.2 Effect of finite size

Linear Elastic Fracture Mechanics (LEFM) theory is valid if the plastic zone at the crack tip is sufficiently small compared to other length scales, such that it is embedded in the elastic singularity zone. In order

for the plastic zone to avoid approaching (or reaching) the outer boundaries of the specimen, the following inequality must be satisfied [1] (see Figure 3.1):

$$a, (W - a), H \geq \frac{4}{\pi}\left(\frac{K}{\sigma_0}\right)^2$$

For fatigue crack growth the thickness is not considered an important factor on the plasticity limitations, as it is for fracture toughness applications [1]. Also, for cyclic loading the size of the plastic zone is slightly reduced compared to the case of static loading [1]. Ideally the NASGRO® equation is supposed to be used strictly under LEFM conditions. For the specimen considered these conditions are slightly compromised for certain load cases and temperatures. However, the conditions are considered to be sufficiently close to apply to the NASGRO® equation, though caution should be taken. If large amounts of plasticity occur during cyclic loading, crack growth rates rapidly increase and exceed expected values. Also, when the plastic zone is too large, failure might be caused by plastic collapse rather than by fatigue.

4 Experimental data

Crack growth is a stochastic process, often showing considerable scatter even in controlled environments. The scatter increases for longer fatigue lives. The crack is initiated where there are stress concentrations due to microstructural inhomogeneities, grain structure influences and/or other influences at micro- or macro scale From this point of view it is important to analyze the scatter in fatigue crack growth rates in a statistical manner.

As mentioned before, at VAC the NASGRO equation is used to characterize the crack growth behavior of a material. The parameters of the NASGRO equation, both for mean behavior and to account for the scatter, are established from the experimental results through a statistical analysis. This chapter explains the experimental set-up and the procedure for establishing the four constants in the NASGRO equation C, n, p and q. Note that the fifth parameter, the crack closure function f, has been established through the FE analyses discussed in detail in the previous chapter.

4.1 Experimental set-up

VAC has performed crack propagation experimental tests of surface crack specimens of cast Inconel 718 at several different temperatures and R-ratios. The experiments produced measured da/dN-data as a function of ΔK, along with threshold values for the different temperatures and R-ratios of interest. See Figure 4.1 for the general set-up.

- The following steps are carried out for the crack propagation testing at VAC:
  - A starter notch is induced with a radius of size of around 0.075-0.5 mm. The notch is machined by spark erosion.
  - The specimen is instrumented by thin measuring wires over the starter notch and at an area that is not affected by the strain fields around the crack but experience the same temperature as the crack during the test (Figure 4.2).
  - A pre-crack is formed by fatigue load at room temperature for $R = 0$ or $R = -1$. Data is recorded for determination of the pre-crack size.
  - The test is carried out at desired temperature and R-ratio and data is recorded for further evaluation. The test is cancelled when the crack is about 2.5 mm due to bending caused by the crack.
  - The specimen is ruptured in a controlled fashion to estimate the fracture toughness (K_c).

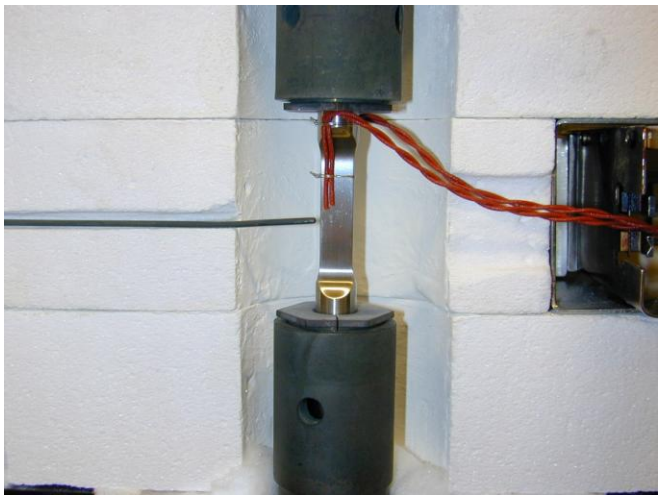

Figure 4.1: Crack propagation set-up at VAC. Crack size detection is made by DC-potential drop.

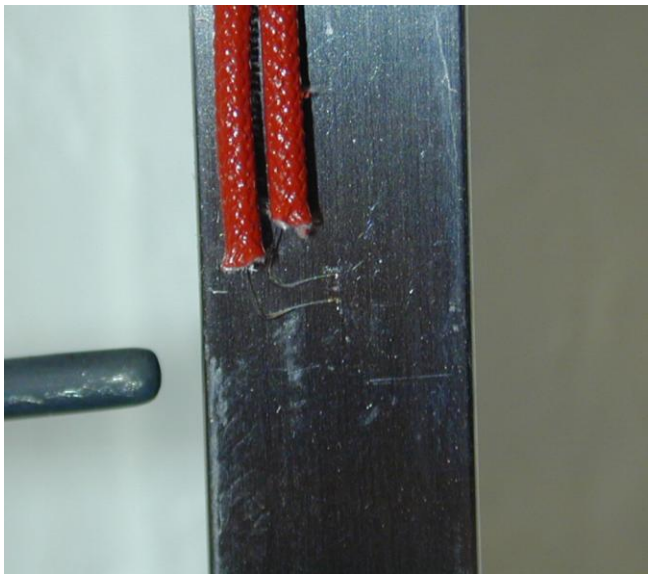

Figure 4.2: A current of 10 A is put through the specimen and the PD-signal is usually between 0.3-1.2 mV.

In the numerical analysis conducted in this thesis only two different temperatures, 20 ^{o}C and 650 ^{o}C, with corresponding *R*-ratios have been considered. The experimental tests conducted at VAC were performed with slightly different maximum loads for each temperature, even for the same *R*-ratio, while the numerically obtained values of f are calculated for only one load case for each *R*-ratio and temperature.

Table 4.1 shows inputs for the experimental tests as well as for the numerical analysis. For a complete curve fit, *f* is required for all different tests, hence certain simplifications are needed. By use of Newman's crack opening function equation (2.8), *f* for the other load cases, are found as:

1. Solve for α from the calculated closure level and corresponding load case, considered in the numerical analysis.
2. Keep α constant for the other load cases, not considered in the numerical analysis, and change the value of σ_{max}/σ_0 accordingly to the desired magnitude of *f*.

Table 4.1: Inputs for experimental tests at VAC

		Experimental testing		Numerical analysis	
T (°C)	R-ratio	Max stress (MPa)	Nr. of tests	Max stress (MPa)	Nr. of tests
20	0	555, 450 450	3	555	1
20	0.5	605, 510 , 510, 510	4	605	1
20	-1	500, 510, 475, 510	4	500	1
650	0	400, 375, 375, 375	4	400	1
650	0.5	475, 400, 400, 425	4	475	1
650	-1	375, 375, 375,375	4	375	1

The threshold value for crack growth is a very important parameter, as described in section 2.2, and it is determined experimentally at VAC by the following steps:

- A pre-crack is induced at room temperature at $R = 0$ or $R = -1$.
- The specimen is subjected to a few thousand compressive load cycles at the test temperature. The compressive load should be at least as large, in relation to the yield strength, as the maximum tensile stress during the creation of the pre-crack. This is to eliminate the influence of a plastic zone with compressive stresses in front of the crack tip.
- The specimen is subjected to cyclic loading at a ΔK slightly smaller than the expected threshold value. If no crack growth is detected after 1000 000 cycles the Δ is increased by 0.2 $MPam^{0.5}$ until crack growth is detected within 1000 000 cycles.
- When crack growth is detected the test is stopped and the specimen is ruptured under controlled conditions to enable accurate measurement of the crack size. Data evaluation is then made using the normal procedures. The threshold value for crack growth is defined as the ΔK giving a crack propagation rate of 10^{-10} m/cycle.

This procedure is not performed as described in ASTM. Instead ASTM suggests a ΔK decreasing method instead. However, this will result in unconservative estimates of the threshold value due to crack tip shielding.

4.2 Least mean square fit to determine C, n, p and q

A curve fit process, based on the experimentally obtained values of *da/dN* versus Δ*K,* is needed to obtain the parameters *C*, *n*, *p* and *q*. Values of the parameters ΔK_{th} and K_c have been obtained by VAC for cast Inconel 718. The method chosen uses a least-squares minimization of error in the log-log domain. By taking the logarithm of equation (2.7), a linear relation with respect to the predictors can be established (for more details see [27]):

$$\log\left(\frac{da}{dN}\right) = \log(C) + n\log\left(\frac{1-f}{1-R}\Delta K\right) + p\log\left(1-\frac{K_{\text{th}}}{\Delta K}\right)$$

$$-q\log\left(1-\frac{K_{\max}}{K_{\text{c}}}\right) \tag{2.14}$$

Written on a general form:

$$Y = \beta_0 + \beta_1 X_1 + \beta_2 X_2 + \beta_3 X_3 \tag{2.15}$$

By identification:

$$\beta_0 = \log(C), \qquad \beta_1 = n, \qquad \beta_2 = p, \qquad \beta_3 = q, \tag{2.16}$$

and:

$$\begin{aligned} Y &= \log\left(\frac{da}{dN}\right), & X_1 &= \log\left(\frac{1-f}{1-R}\Delta K\right), \\ X_2 &= \log\left(1-\frac{K_{\text{th}}}{\Delta K}\right), & X_3 &= \log\left(1-\frac{K_{\max}}{K_{\text{c}}}\right), \end{aligned} \tag{2.17}$$

Applying equation (2.14) for each experimental data point and writing on matrix form gives:

$$y = X\beta \tag{2.18}$$

where:

$$y = [Y_i] \tag{2.19}$$

$$X = \left[1\ X_{1,i}\ X_{2.i}\ X_{3,i}\right] \tag{2.20}$$

$$\beta = [\beta_0\ \beta_1\ \beta_2\ \beta_3]^T \tag{2.21}$$

and $i = 1, \ldots, n$ where n is the number of data points. The coefficients are estimated by least squares, thus minimizing the sum of squares of the residuals which is equivalent to solve the equations:

$$X^T y = X^T X\beta \tag{2.22}$$

If the inverse of $(X^T X)$ exists then the coefficients are obtained by:

$$\beta = (X^T X)^{-1} X^T y \tag{2.23}$$

With the above explained procedure the parameters *C*, *n*, *p* and *q* can be obtained. However, an option is to move the terms $p \ln\left(1 - \frac{K_{\text{th}}}{\Delta K}\right)$ and $-q \ln\left(1 - \frac{K_{\max}}{K_c}\right)$ to the left hand side of equation (2.1) using fixed, standard values of *p* and *q,* and making the least square fit with respect to only *C* and *n*. This is a more common procedure since experimental data is lacking in the two extreme regions, corresponding to parameters *p* and *q*. Both procedures are applied and compared in the following sections to check which gives the best prediction of crack propagation rates.

4.3 Results

Figure 4.3 shows the *da/dN*-data versus (a) Δ*K* and (b) $\Delta K_{\text{eff}} = \frac{1-f}{1-R}\Delta K$ for T = 20 °C. As can be seen, the *da/dN*-data merges quite well if plotted against ΔK_{eff}, indicating the validity of Elber's assumption and the numerically obtained *f*.

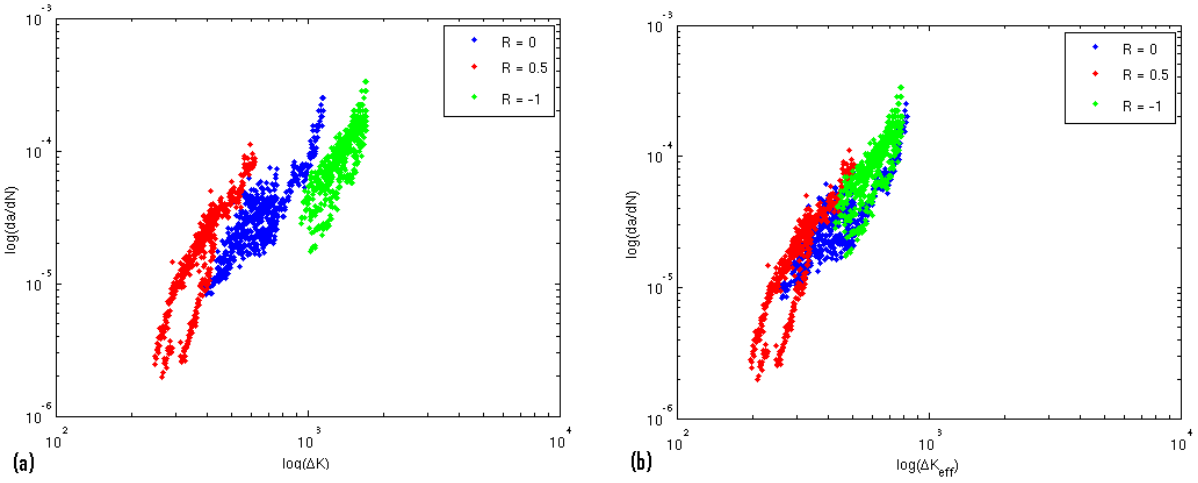

Figure 4.3: Experimental data, T = 20 °C (a) *da/dN* versus Δ*K*, (b) *da/dN* versus ΔK_{eff}.

Figure 4.4 shows the corresponding plots for T = 650 °C. Also here the data merges quite well, however not as good as for T = 20 °C.

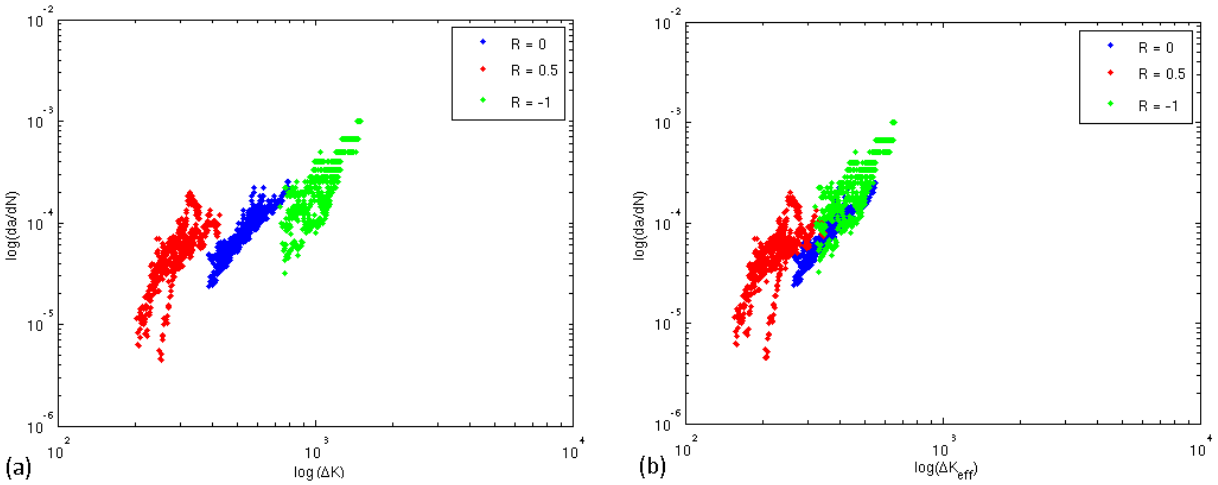

Figure 4.4: Experimental data, T = 650 °C (a) *da/dN* versus ΔK, (b) *da/dN* versus ΔK_{eff}.

Figure 4.5 shows a generated curve fit with ΔK_{eff} ranging from ΔK_{th} to $K_{max} = K_c$ for (a) when letting p and q be free and (b) locking them as $p = 0.25$ and $q = 0.75$. The two procedures clearly give different estimation of the crack propagation rates. However, in both cases it is evident that the experimental data mainly covers the Region II of the crack propagation rate curve.

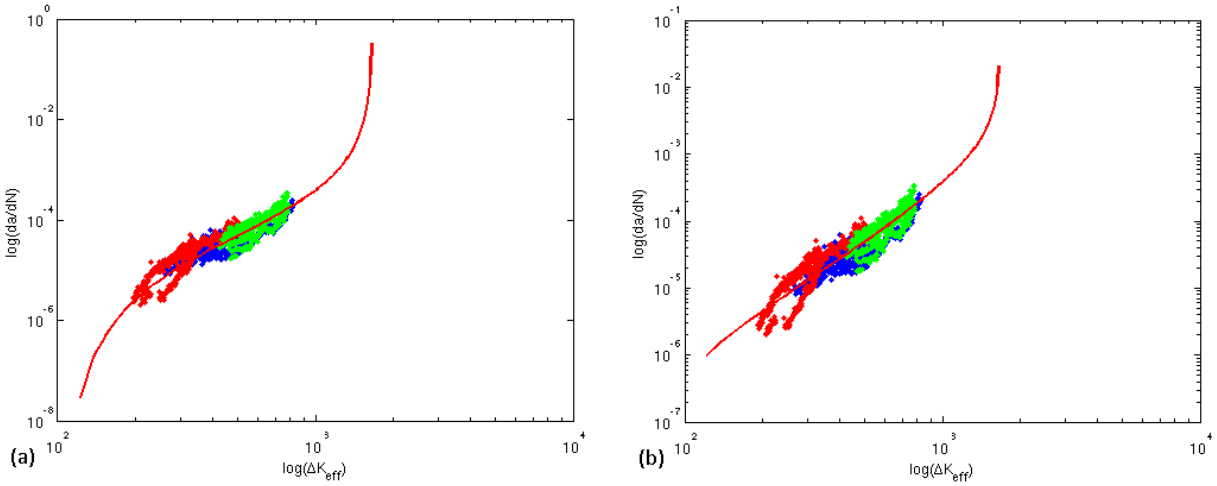

Figure 4.5: Generated curve fit with ΔK_{eff} ranging from ΔK_{th} to $K_{max} = K_c$ for (a) when letting p and q be free and (b) setting p = 0.25 and q = 0.75.

The obtained values of the fitted parameters for the respective temperature are shown in Table 4.2 for the two proposed methods as well as for VAC's current method (where all five parameters are obtained through curve fitting). The parameters C and n have been scaled. Note that, there are other parameters with differing values between the methods. A clear difference of C and n can be seen for the two

proposed methods. The acquainted reader of fracture mechanics will, by studying the numbers when letting *p* and *q* be free, observe unusually high values. Recall that *p* and *q* control the shape of the asymptote in the threshold and critical crack growth region, respectively. Thus, the two methods show very different behavior for the threshold crack growth region as is evident in Figure 4.5.

Table 4.2: The fitted parameters *C*, *n*, *p* and *q* for the two temperatures considered, and both proposed methods as well as VAC's current method. Top: *p* and *q* free, middle: *p* and *q* locked, bottom: VAC's current method. The parameters *C* and *n* have been scaled so that *n* = 1.

	Proposed method (p and q free)	
	T = 20 °C	T = 650 °C
C	3,37E-08	6,13E-07
n	1	1
p	2,9042	2,7386
q	1,6647	1,119

	Proposed method (p and q locked)	
	T = 20 °C	T = 650 °C
C	1,07E-11	1,38E-10
n	1	1
p	0,25	0,25
q	0,75	0,75

	VAC's current method	
	T = 20 °C	T = 650 °C
C	9,17E-14	5,94E-13
n	1	1
p	0,25	0,25
q	0,75	0,75

4.4 Discussion

An important question arises regarding how reasonable it is to obtain *p* and *q* from a least square fit, when there is a severe lack of data in these regions, as illustrated in Figure 4.5. By inspecting Figure 4.5, one can argue that the curve better follows the experimental data when letting *p* and *q* be free. However, it is hard to determine which fit is the most accurate with simple visual inspection of these particular plots. Further experimental data is obviously needed in the threshold crack growth region to determine the accuracy of the fit in that region. When conducting tests for determining threshold levels, the crack should be allowed to grow longer, i.e. conduct a complete crack propagation test, in order to obtain more data in the low stress intensity regions. Additional data should also be obtained in the high stress intensity regions to be able to determine the accuracy of *q*.

For T = 650 ^{o}C the *da/dN* data for different *R*-ratios did not merge as well as for T = 20 ^{o}C when plotting against ΔK_{eff}. One reason may be that other closure mechanisms than PICC have increased influence on the crack closure level at this temperature. However, the reason for the unsatisfying curve fit at this temperature is uncertain and should be investigated further.

5 Evaluation of the proposed method

In this section a statistical evaluation of the life predictions are carried out for the two proposed methods (*p* and *q* free and locked respectively) and are compared to the current method used at VAC. A discussion of what is needed in the future to more accurately describe the crack propagation behavior is also included.

5.1 Crack propagation analysis

The crack propagation analysis is conducted with the NASGRO® software using the here established parameters *C*, *n*, *p* and *q* as well as the estimated values of α and $\sigma_{\max}/\sigma_0$. Further, the fracture toughness, K_c, and the threshold stress intensity range, ΔK_{th}, is supplied. The threshold level as *R* approaches 1 , ΔK_1, is assigned in the NASGRO® software and is given by [9]:

$$\Delta K_1 = \Delta K_0 (1 - A_0)^{(1+C_{\text{th}}^p)}$$

where ΔK_0 is the threshold value at $R = 0$ and A_0 is given by equation (2.9). The constant C_{th} can be used to model the threshold value for different degrees of crack closure. In this thesis it will be set to 0 leading to a more conservative prediction.

One way to determine the validity of the model is to compare the predicted life (P) with the actual life (A) observed in the experimental testing. For each case the actual life over the predicted life (A/P) is calculated. An A/P-value of around 1 is obviously desirable, a value less than one implies a non-conservative estimate of life and a value above one implies a conservative estimate of life. Comparing the predicted life using VAC's current method will reveal if the more thorough analysis, used in the proposed method, will increase the accuracy of the life predictions.

5.2 Results

To illustrate the accuracy of the predicted lives, Minitab probability plots are used. They show the probability distribution of acquired A/P-values. If the method used for life predictions is good, it should have an A/P of 1 at 50% probability. The distribution should also deviate from A/P = 1 as little as possible, i.e. have a vertical shape. Figure 5.1 shows the Minitab probability plot for the proposed method (*p* and *q* free) versus the current method used at VAC. Figure 5.2 shows the proposed method (*p* and *q* free) versus the proposed method (*p* and *q* locked).

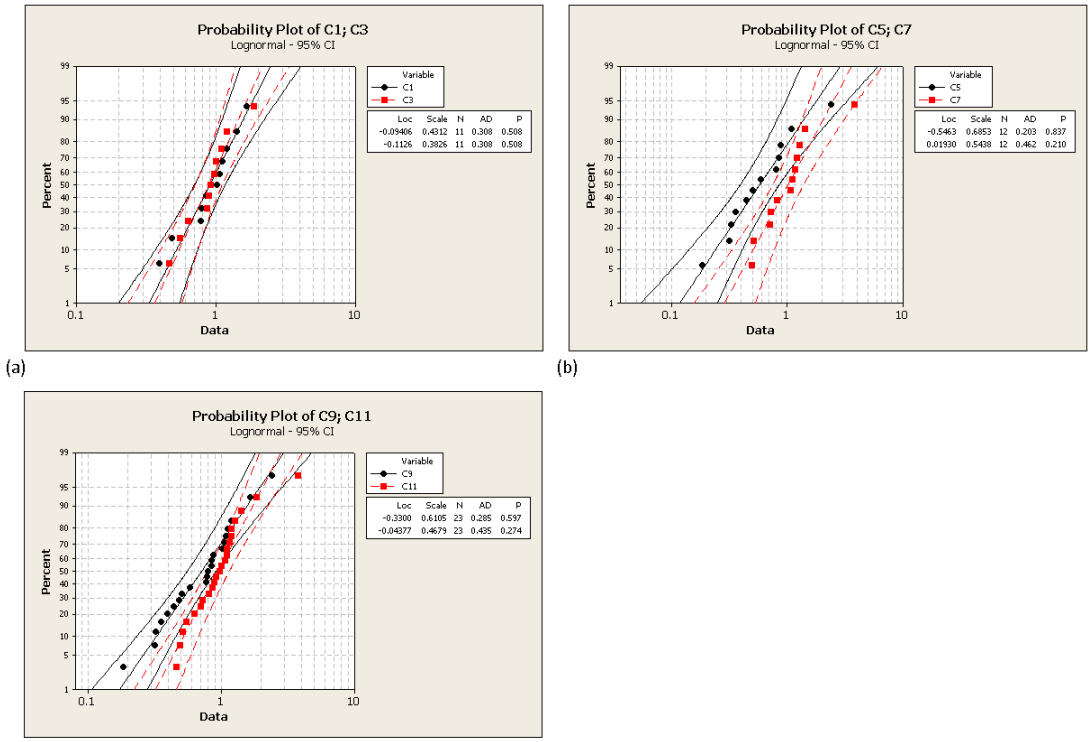

Figure 5.1: Minitab probability plot; the proposed method (*p* and *q* free) (black) versus current method used VAC (red). (Vertical axis: probability, Horizontal axis: A/P-value).

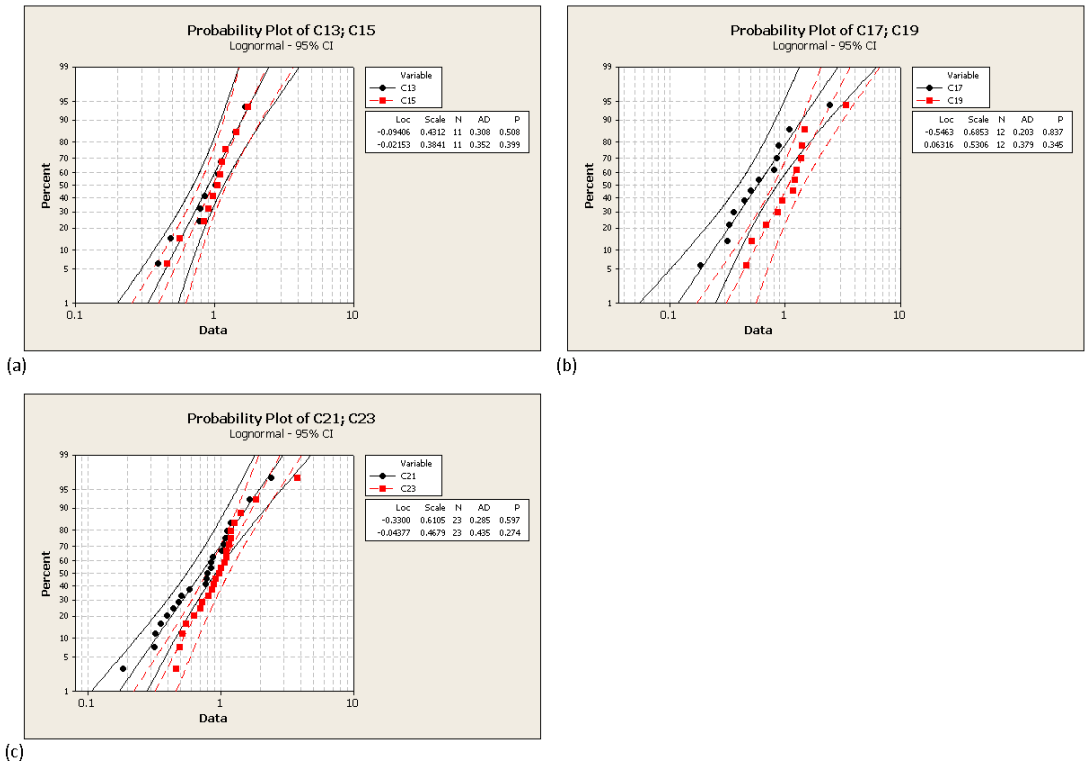

Figure 5.2: Minitab probability plot; the proposed method (*p* and *q* locked) (black) versus current method used VAC (red). (Vertical axis: probability, Horizontal axis: A/P-value).

5.3 Discussion

For T = 20 °C both proposed methods as well as the current method used at VAC show good life predictions. However for T = 650 °C all three methods show somewhat less accurate predictions. However, the proposed method (*p* and *q* locked) and the current method used have an A/P-value of 1 at 50% probability which it should have. This is not the case for the proposed method (*p* and *q* free). The proposed method shows similar results as the current method used at VAC, but with slightly lower scatter.

A few reasons for the unsatisfactory results are discussed below. The pre-crack length of the test specimens varies between 0.5 and 1 mm and is grown to between 2 and 3 mm. It is important to investigate if the assumed LEFM conditions are valid for these sizes. There are two limitations of a short crack modeling: 1) microstructurally and mechanically small cracks cannot be described by linear elastic fracture mechanics (LEFM) and 2) the threshold behavior may be very different for microstructurally small cracks as compared to long cracks from which material data are obtained [28]. Continuum theory can generally be applied on cracks with length greater than 10 grain sizes [28] and Inconel 718 has a grain size of 5 – 40 µm [29], leading to that the required crack size would be 50 – 400 µm. Therefore, all cracks can be considered not being micro structurally small. However, the crack can initially be considered as mechanically short (100 µm to 1 mm) and during its growth the crack can be considered as mechanically long [2]. Continuum theory can be applied on mechanically short crack, but exhibit different mechanical behavior than longer cracks. Typically, short cracks grow faster than long cracks at the same ΔK-value, especially near the threshold level [2]. This can have a large effect on the errors in the predicted lives, especially for the cracks starting at approximately 0.5 mm.

The main problem encountered when analyzing the experimental data available, is the fact that the data almost only covers the linear part (Region II). This will obstruct the curve fitting procedure and limit the possibility to acquire good values of *p* and *q* in the NASGRO® equation. As discussed in section 4.4, more data should be obtained near the threshold value as well as for high stress intensity ranges.

It should also be noted that there is an inherent scatter in the testing (secondary bending, crack surface irregularities etcetera). A remark on the threshold value is worth a mention here; it is a complicated procedure to obtain the threshold value, as it is dependent on the *R*-ratio and on how the test is conducted . During the crack propagation analysis it was observed that the predicted lives where highly dependent on the choice of the threshold level, ΔK_{th}. Varying ΔK_1 by ±10%, the predicted life changes between 10% and 20%. The value of *p* in the NASGRO® equation clearly plays an important role for the effect of the threshold value. It is thus very important to get a good estimate to be able to reduce the errors in life predictions.

Even though the proposed method did not improve the life predictions, this thesis provides a better physical understanding of the crack propagation phenomenon. It is now also possible to expand the model for different geometries, for example a through crack, which might have different closure levels, resulting in more accurate life predictions. The thesis also provides a basis for further improvements of the crack propagation modeling at Volvo Aero.

6 Summary and Conclusions

This master's thesis examines whether it is possible to make more accurate life predictions of aircraft engine components by employing a more physical approach to identifying parameters in crack propagation models as compared a pure curve fit method. The objective was to statistically evaluate the predictions of these two methods and compare to experimental data. The physics-based method shows promise, as the predicted lifetime on average is similar to the pure curve fit method with slightly lower scatter of predicted versus actual lives. The model can be expanded for different geometries with different crack closure levels resulting in more accurate life predictions.

Some other conclusions from this thesis are:

- With the model and crack propagation scheme used in this thesis, an unequivocal value of α cannot be directly established. A further understanding of this parameter is desired.
- Crack closure and thereby α do not seem to have a direct relation to temperature.
- Consideration of the maximum load applied at experimental testing is necessary to avoid a large effect of the finite size geometry. This is especially important when evaluating crack closure.
- The crack opening along the crack front for this specimen starts in the interior and then moves towards the free surface for $R = 0$, $R = 0.5$ and $R = -1$. This variation does not considerably affect the weighted average of f, since the amplified region only stretches up to an angle of approximately 10^{o} from the free surface.

For the future:

- Additional experimental crack growth rate data in region I and III is needed to get more accurately fitted constants.
- In addition to the lack of crack growth rate data in region I, there are also uncertainties in the threshold stress intensity range. Additional and more thorough measurements of the threshold level should be obtained.
- The numerically established closure levels should be confirmed experimentally to validate that the obtained values are reasonable.

7 References

1. Dowling, N.E., "Mechanical Behavior of Materials – Engineering methods for Deformation, Fracture, and Fatigue", 2007, Third Edition, Pearson Education International, USA.
2. T.L. Anderson, "Fracture Mechanics – Fundamentals and applications", 1991, Taylor & Francis group, Florida, USA.
3. Suresh. S., "Fatigue of Materials", 1991, Cambridge University Press, Cambridge, UK.
4. Paris, P.C. and Erdogan, F., "A Critical Analysis of Crack propagation Laws", *Journal of Basic Engineering*, 1960, **85** pp. 528-534.
5. McClung, R.C., Sehitoglu, H., "On the finite element analysis of fatigue crack closure – 1 Basic modeling issues", 1989, *Engineering Fracture Mechanics,* **33**, pp. 237-252.
6. Ritchie R.O. and Suresh S., "Some considerations on fatigue crack closure at near-threshold stress intensities due to fracture surface morphology", 1981, *Metal Trans,* **13A.** pp. 937–40.
7. Elber, W.,"Fatigue crack closure under cyclic tension", 1970, *Engineering Fracture Mechanics*, **2**(1), pp. 37-44.
8. Newman, J.C., "A Crack Opening Stress Equation for Fatigue Crack Growth". *International Journal of Fracture*, Mars 1984, **24**(3), pp. R131-R135.
9. NASGRO® Manual, Version *6.2*, 2011.
10. Borrego L.F.P., Antunes F.V., Costa J.D., Ferreira, J.M., "A numerical study of fatigue crack closure induced by plasticity", 2004, *Fatigue & Fracture of Engineering Materials & Structures,* **27**(9), pp. 825 – 835.
11. Roychowdhury, S., Dodds, R.H., "Thee-dimensional effects on fatigue crack closure in the small-scale yielding regime – a finite element study". January 2003, *Fatigue & Fracture of Engineering Materials & Structures*, **26**(8), pp. 663-673.
12. Roychowdhury, S., Dodds, R.H., "A numerical investigation of 3D small scale yielding fatigue crack growth", *Engineering Fracture Mechanics,* **2003, 70**, pp. 2363–83.
13. Antunes , F.V., Rodrigues D.M., "Numerical simulation of plasticity induced crack closure: Identification and discussion of parameters", Nov 2008, *Engineering Fracture Mechanics, **75**,* pp. 3101-3120.
14. ANSYS Manual, release 12.1, 2009.
15. Hou, Chien-Yuan., "Three dimensional finite element analysis of fatigue crack closure behavior in surface flaws", 2004, *International journal of fatigue.* **26,** pp. 1225-1239.
16. Skinner, J.D., and Daniewicz, S.R., "Simulation of plasticity induced fatigue crack closure in part-through cracked geometries using finite element analysis", 2002, *Engineering Fracture Mechanics,* **69**, pp. 1-11.
17. McClung, R.C., Thacker, B. H and Roy, S., "Finite element visualization of fatigue crack closure in plane stress and plane strain", 1991, *International Journal of Fracture,* **50**, pp. 27-49.
18. Kiran Solanki, S.R. Daniewicz, J.C. Newman Jr., "Finite element analysis of plasticity-induced fatigue ecrack closure: an overview", 2004, *Engineering Fracture Mechanics,* **71**. pp. 149–171.
19. Zhang, J. Z. and Bowen, P., "On the finite element simulation of three-dimensional semi-circular fatigue crack growth and closure". 1998, *Engineering Fracture Mechanics,* **60**, pp. 341-360.
20. de Matos P.F.P. and Nowell D., "Numerical simulation of plasticity-induced fatigue crack closure with emphasis on the crack growth scheme: 2D and 3D analyses", 2008, *Engineering Fracture Mechanics*, **75**, pp. 2087–2114.

21. McClung, R.C., Sehitoglu, H, "On the finite element analysis of fatigue crack closure – 2. Numerical results", 1989, *Engineering Fracture Mechanics,* **33**, pp. 253-272.
22. Ellyin F. and Ozah. F, "3D modelling of plasticity induced fatigue crack closure-effect of material constitutive relations", 2010, *Engineering Fracture Mechanics*, **77**, pp. 1693-1707.
23. Wu J, Ellyin F., "A study of fatigue crack closure by elastic–plastic finite element analysis for constant-amplitude loading", 1996, *International Journal of Fracture,* **82**(1). pp. 43–65.
24. Putra IS and Schijve J. "Crack opening stress measurements of surface cracks in 7075-T6 aluminum alloy plate specimen through electron fractography", 1992, *Fatigue and Fracture Engineering Materials and Structures*, **15**(4), pp. 323–38.
25. McDonald V, Daniewicz SR., "An experimental study of the growth of surface flaws under cyclic loading: experimental uncertainty, aspect ratio evolution, and the influence of crack closure", 2001, *ASTM STP* 1406, pp. 381-96.
26. Newman, J.C., Raju, I.S., "An empirical stress intensity factor equation for the surface crack", 1981, *Engineering Fracture Mechanics,* **15**(1-2), pp. 185-92.
27. Veitch, R., Zuyev, S., Muratov, A., "Introduction to Probability and Mathematical Statistics VLE Study guide", March 2012, Chalmers University of Technology, Gothenburg, Sweden.
28. Mark A. James, David S. Dawicke, Matthew B. Brzowski, Ivatury S. Raju, Kenny B. Elliott, and Charles E. Harris, "Fracture Mechanics Analysis of LH2 Feed Line Flow Liners", 2006, http://wayback.archive-it.org/1792/20100127101936/http://hdl.handle.net/2060/20060020274.
29. Harris, C. E., "Orbiter LH 2 Feedline Flowliner Cracking Problem", NASA/TM- 2005 - 213787/Version 1.0, NESC-RpP-04-ll/04-004-E, July 2005.

Appendix A
- Results: Crack closure levels from FE-analysis

Figures A.1 – A.6 show the numerically established values of the crack opening function, f, for all temperatures and R-ratios considered in the FE-analysis.

Figures (a) – (d) show f as a function of crack growth increment, Δa, at different degrees along the crack front and figures (e) show stabilized values of f as a function of φ.

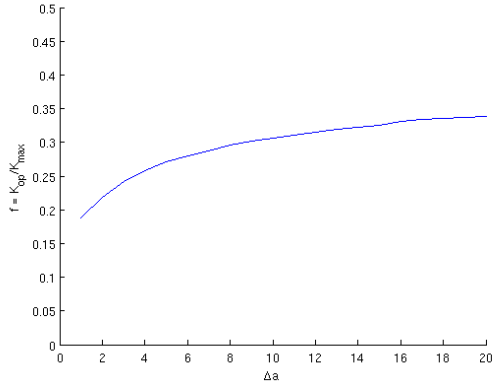

a) $\boldsymbol{\phi = 0^o}$**.**

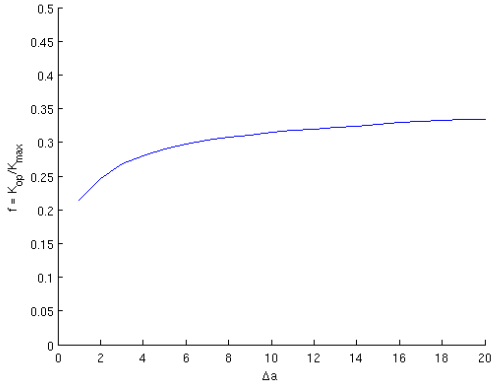

b) $\boldsymbol{\phi = 5.4^o}$**.**

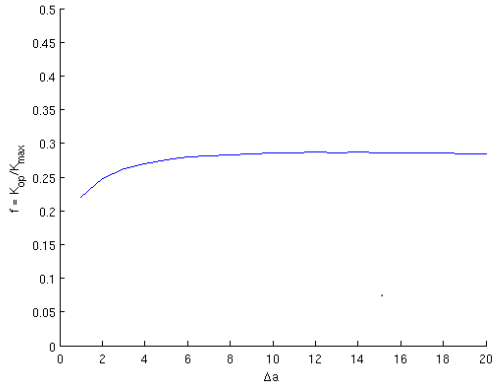

c) $\boldsymbol{\phi = 45^o}$**.**

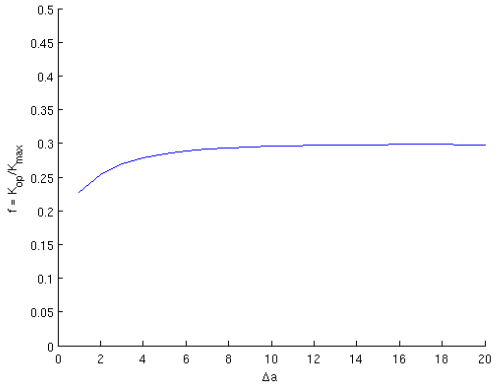

d) $\boldsymbol{\phi = 90^o}$**.**

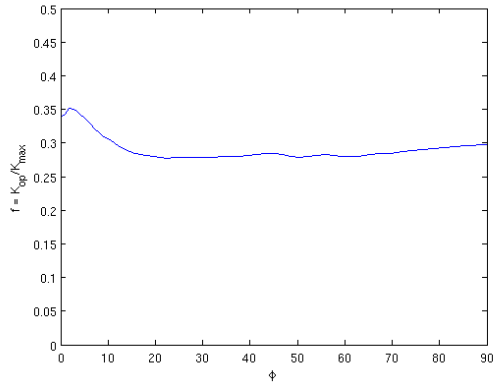

e) $\boldsymbol{f(\phi)}$**.**

Figure A.1: T = 20 °C, *R* = 0, L_e = 0.05 mm.

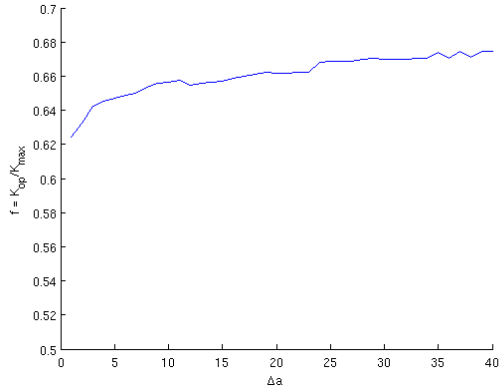

a) $\boldsymbol{\phi = 0^o}$**.**

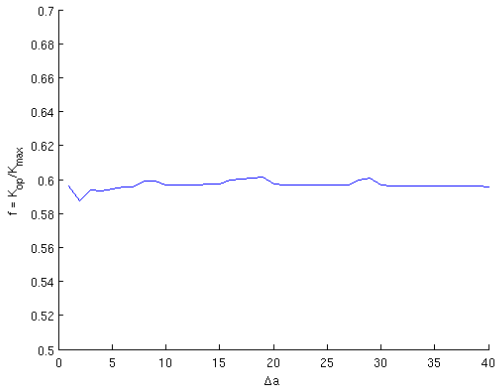

b) $\boldsymbol{\phi = 5.4^o}$.

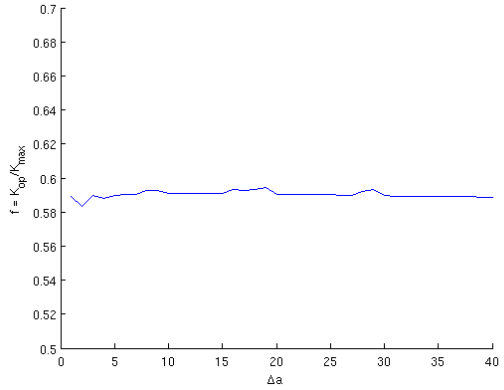

c) $\boldsymbol{\phi = 45^o}$.

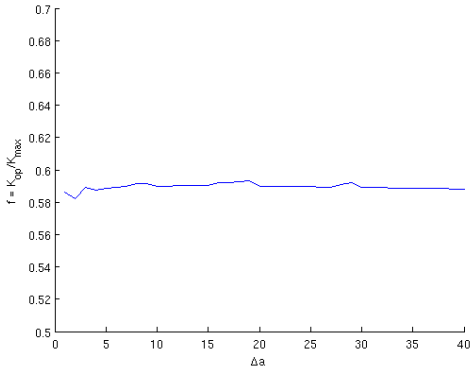

d) $\boldsymbol{\phi = 90^o}$**.**

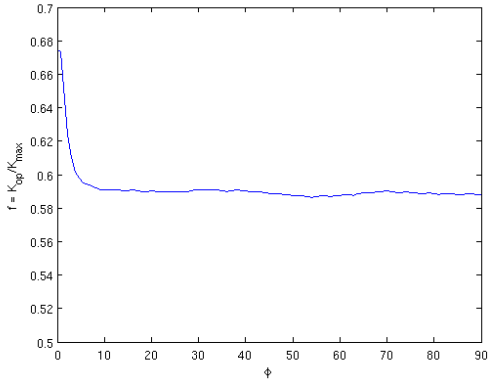

e) $\boldsymbol{f(\phi)}$.

Figure A.2: T = 20 °C, *R* = 0.5, L_e = 0.025 mm.

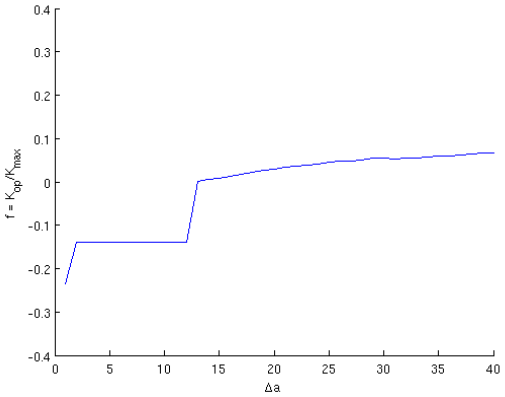

a) $\boldsymbol{\phi = 0^o}$.

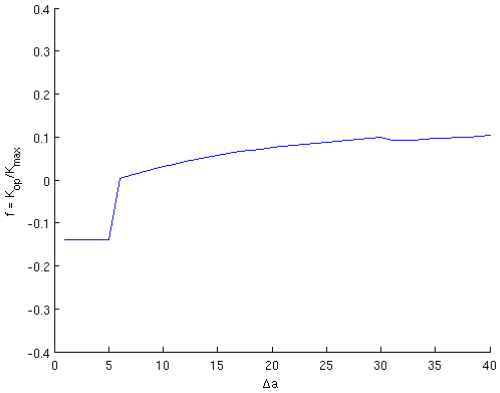

b) $\boldsymbol{\phi = 5.4^o}$.

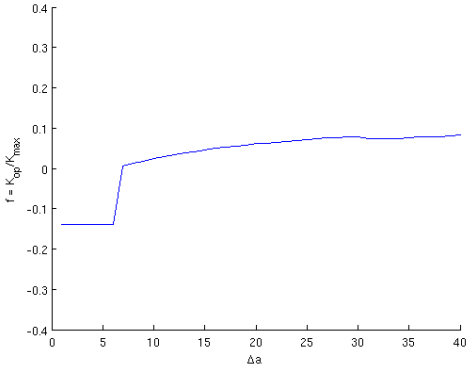

c) $\boldsymbol{\phi = 45^o}$.

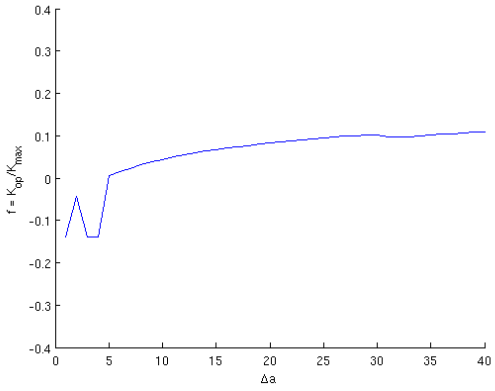

d) $\boldsymbol{\phi = 90^o}$.

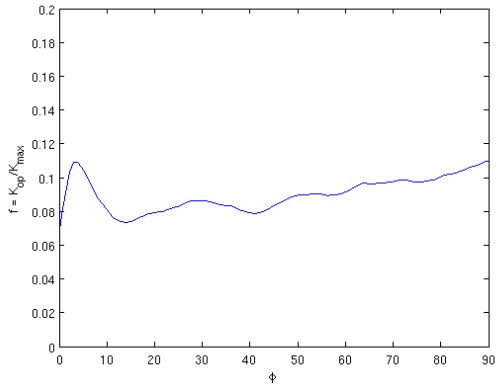

e) $\boldsymbol{f(\phi)}$.

Figure A.3: T = 20 °C, *R* = -1, L_e = 0.025 mm.

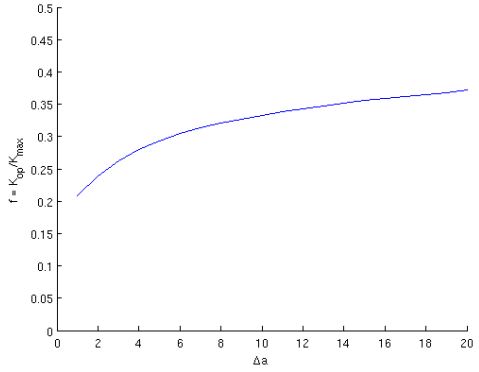

a) $\boldsymbol{\phi = 0^o}$

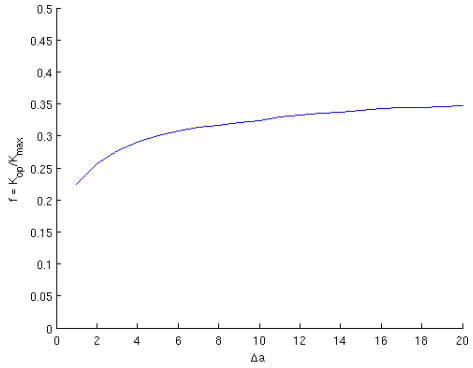

b) $\boldsymbol{\phi = 5.4^o}$

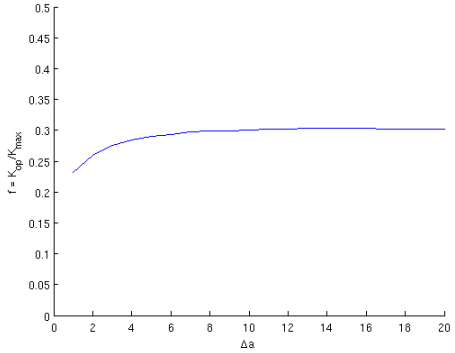

c) $\boldsymbol{\phi = 45^o}$**.**

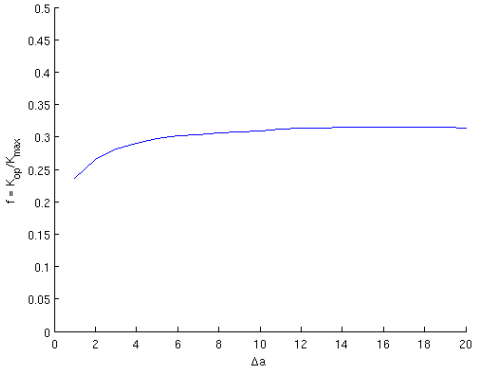

d) $\boldsymbol{\phi = 90^o}$.

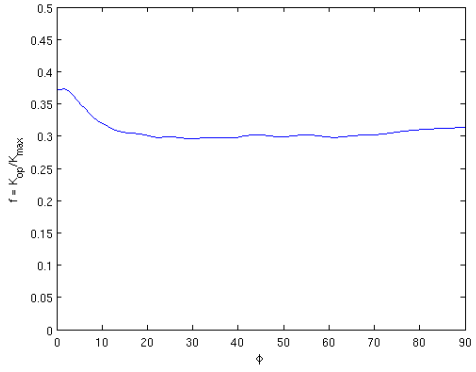

e) $\boldsymbol{f(\phi)}$.

Figure A.4: T = 650 °C, *R* = 0, L_e = 0.05 mm.

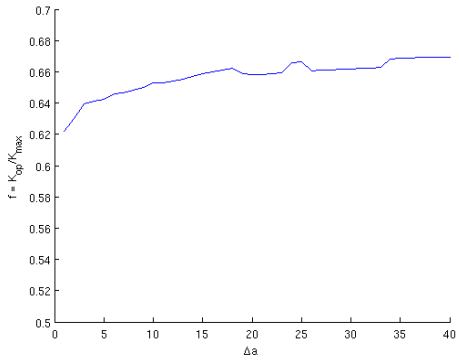

a) $\boldsymbol{\phi = 0^o}$.

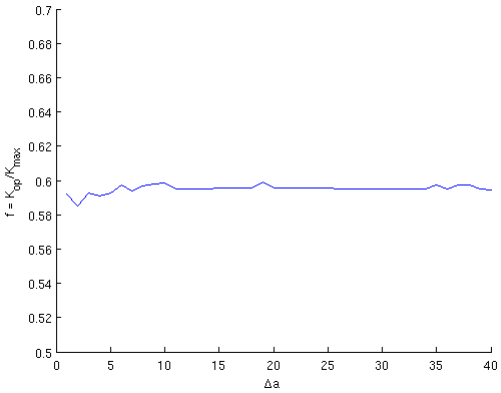

b) $\boldsymbol{\phi = 5.4^o}$.

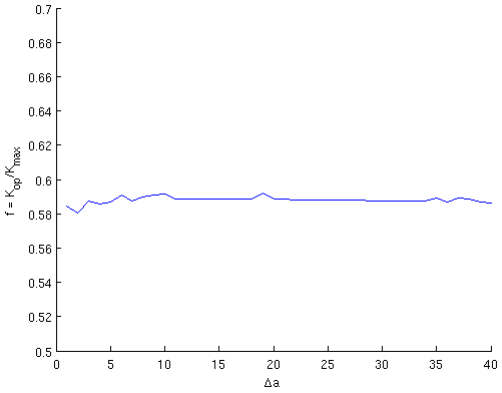

c) $\boldsymbol{\phi = 45^o}$.

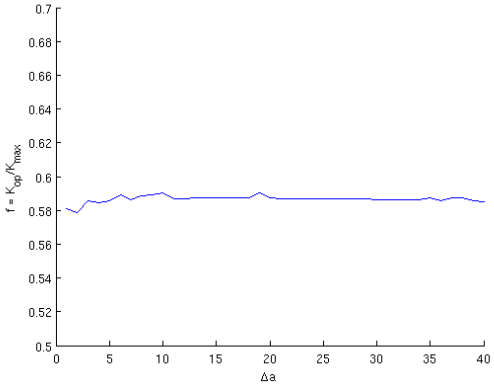

d) $\boldsymbol{\phi = 90^o}$.

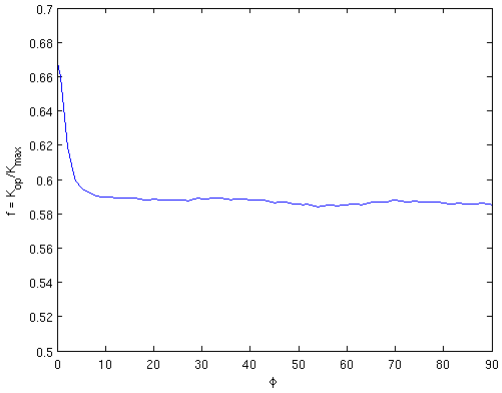

e) $\boldsymbol{f(\phi)}$.

Figure A.5: T = 650 ^{o}C, *R* = 0.5, L_e = 0.025 mm.

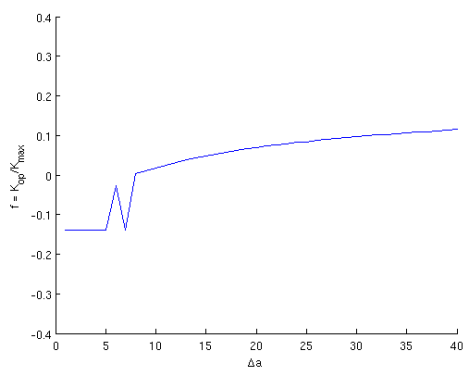

a) $\boldsymbol{\phi = 0^o}$.

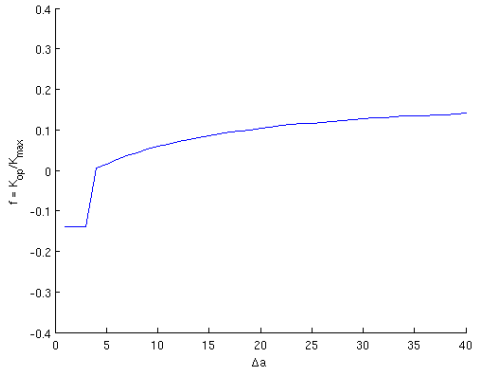

b) $\boldsymbol{\phi = 5.4^o}$.

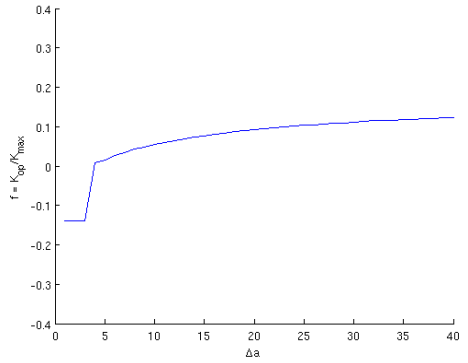

c) $\boldsymbol{\phi = 45^o}$.

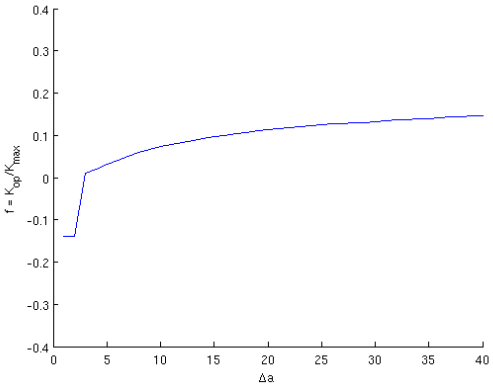

d) $\boldsymbol{\phi = 90^o}$

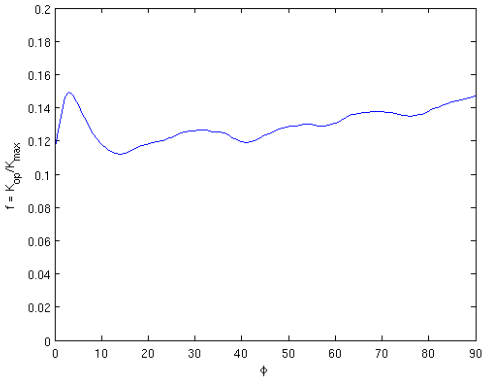

e) $\boldsymbol{f(\phi)}$.

Figure A.6: T = 650 ^{o}C, *R* = -1, L_e = 0.025 mm.

Appendix B
-Newman's crack opening function

Figure B.1 – B.2 shows Newman's crack opening function, f, versus plane stress/strain constraint factor, α, for the values of σ_{max}/σ_0 considered in the FE-analysis.

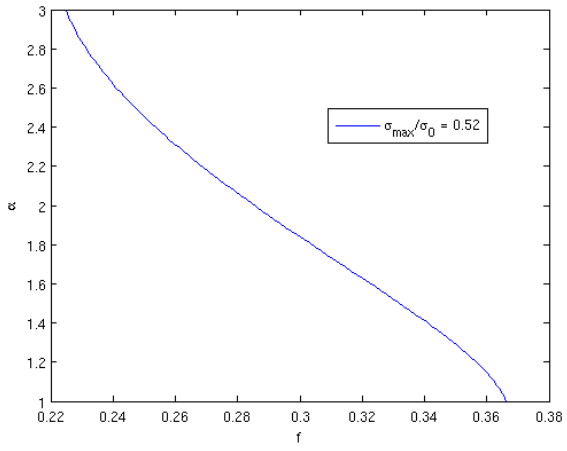

a) R = 0, σ_{max}/σ_0 = 0.52.

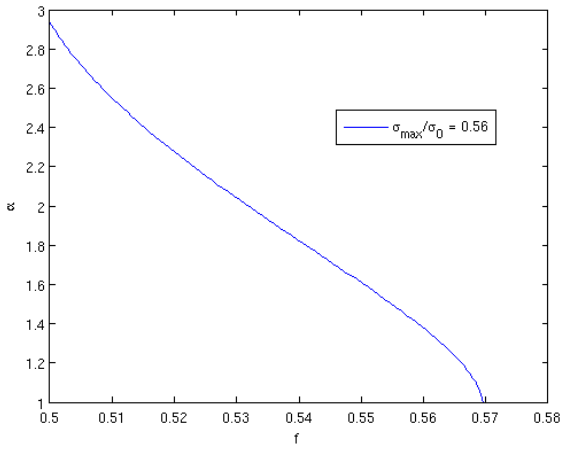

b) R = 0.5, σ_{max}/σ_0 = 0.56.

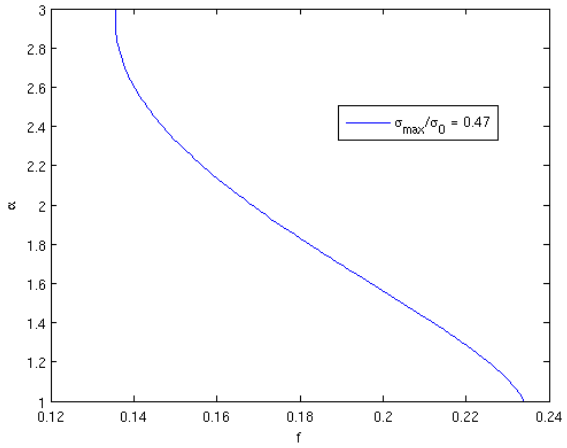

c) R = -1, σ_{max}/σ_0 = 0.47.

Figure B.1: Crack opening function, f, versus plane stress/strain constraint factor, α.

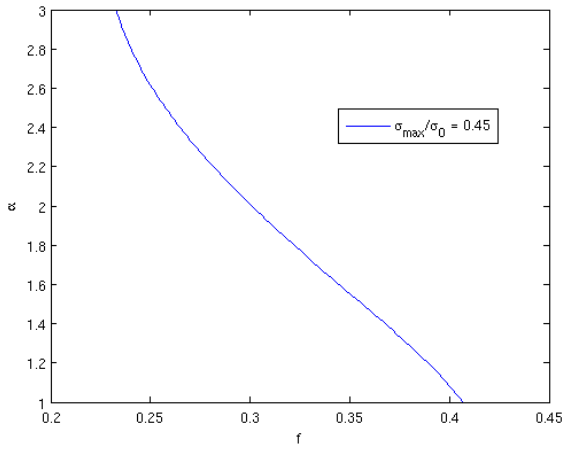

a) R = 0, σ_{max}/σ_0 = 0.45.

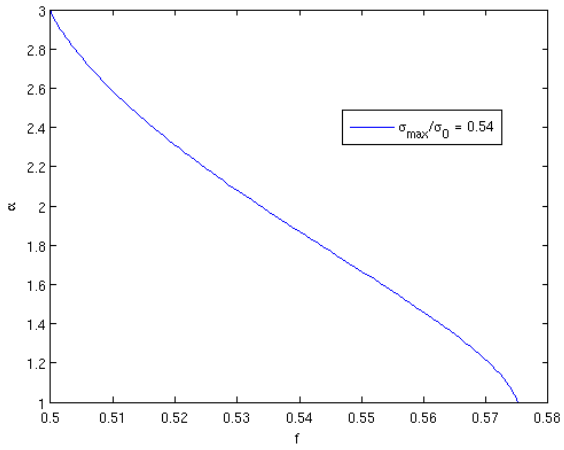

b) R = 0.5, σ_{max}/σ_0 = 0.54.

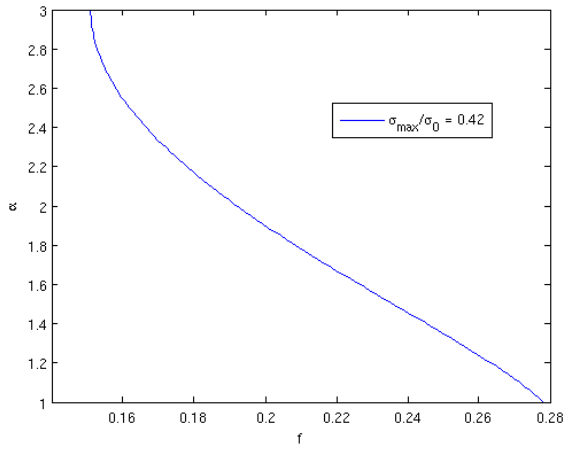

c) R = -1, σ_{max}/σ_0 = 0.42.

Figure B.2: Crack opening function, f, versus plane stress/strain constraint factor, α.

Appendix C
- Comments on mesh building

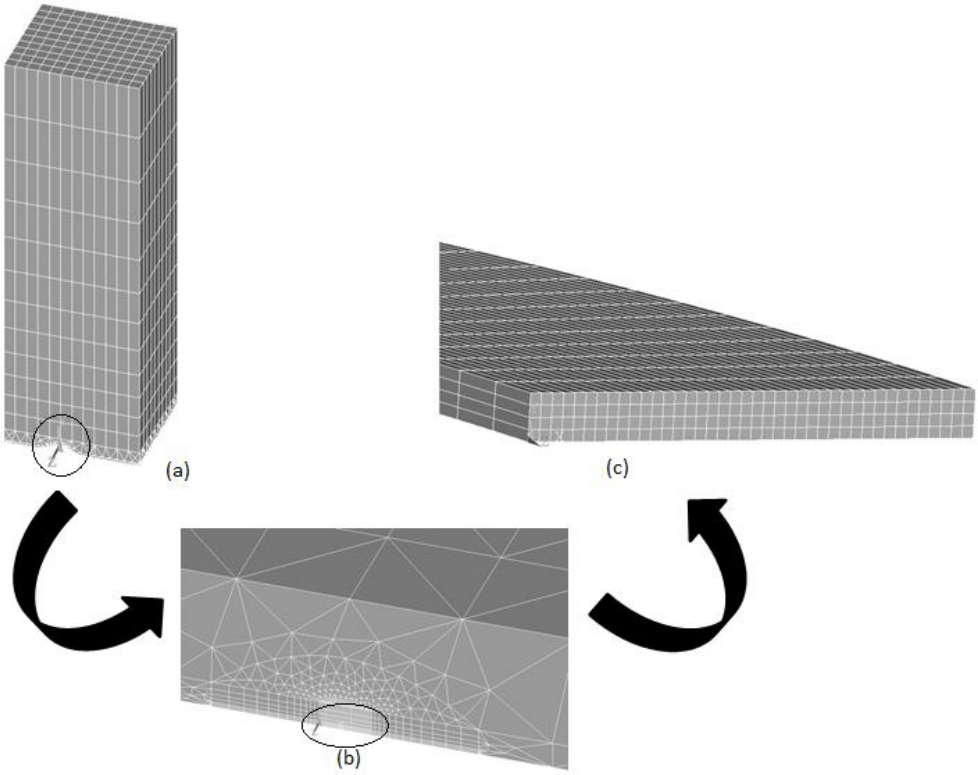

Figure C.1: Typical finite element mesh (scaled): (a) Overall view (b) transition from near crack tip domain to outer domain (c) Close up view at crack front in propagation direction.

In the circumferential direction (φ-direction in Figure C.2) there are desires on the element size to capture the variation of the opening levels as well as on computational reliability. Hou [15] states that the stress variation is much milder in this direction compared to the radial direction with about 10 % variation between plane strain and plane stress; hence a larger ratio can be used. If the crack geometry is balanced then ΔK should be close to constant in the circumferential direction. As can be seen in Figure 3.2 (c) a significant large aspect ratio has been used compared to the length in the radial direction (L_e). his has been shown to have negligible effect on the closure levels. Figure C.3 compares two separate

results from analyses with aspect ratios of approximately 20 and 5, respectively. By allowing larger aspect ratio, the number of elements decreases drastically meaning a huge difference in computational time.

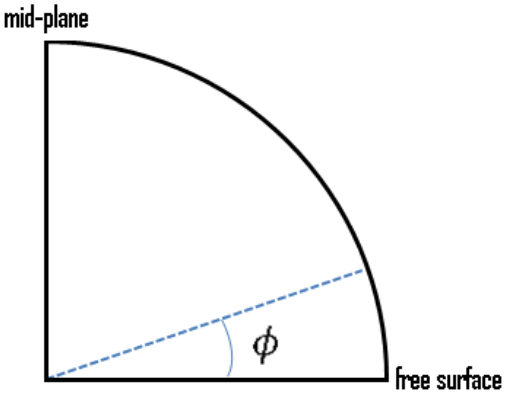

Figure C.2: Circumferential direction in the crack plane. φ varies from 0 to 90 degrees with 0 degrees at the free surface.

It is of great importance to keep the number of elements low as well as having a smooth transition from the fine mesh at the crack tip to the coarse mesh. A linear hexahedral element type is used at and around the crack tip according to the cubic element in Figure C.4 (a). This implies that a 9-noded tetrahedron element should be used for transition with a layer of pyramidal elements between the hexahedral and tetrahedral elements, as illustrated in Figure C.4 (b). A transitional mesh consisting of 4-noded linear tetrahedral elements has been used according to the red element in Figure 3.3 (a), regardless of the violation of the C^0 continuity as illustrated in Figure C.4 (a). As can be seen the common surface between the hexahedral and tetrahedral elements has a non-matching mesh. Using 4-noded linear tetrahedron will significantly reduce the degrees of freedom leading to that this meshing issue is a trade-off between loss of accuracy and computational effort.

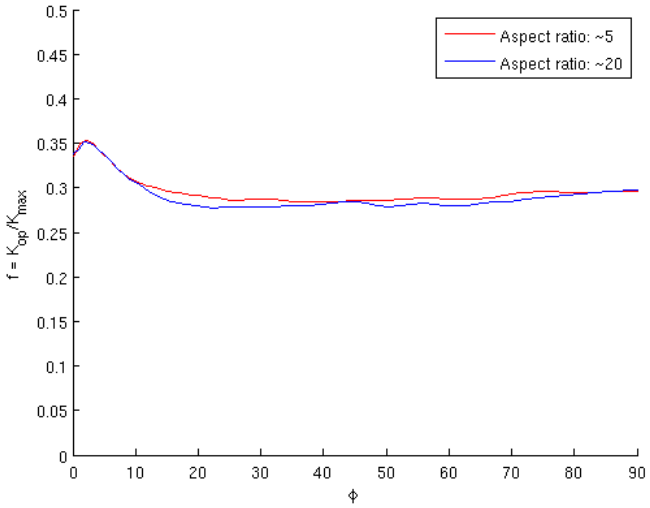

Figure C.3: Effect of increasing the aspect ratio in the circumferential direction of the elements along the crack front. Aspect ratio of approximately 20 versus approximately 5.

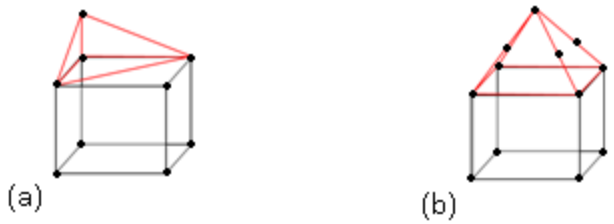

Figure C.4: Elements in the transitional mesh, (a) non-matching mesh between hexahedral and tetrahedral elements at the common surface thus violating C^0 continuity, (b) consistent transition between hexahedral and pyramidal elements.

Figure C.4 shows the difference in predicted opening levels by using linear (without mid-nodes) and non-linear quadratic (with mid-nodes) elements in the transitional part. It is clear that using quadratic elements has a marginal effect on the closure levels. In this work the analyses have been made by linear tetrahedrons for above discussed reasons but it is recommended that in forth coming analysis, especially if a stress analysis is to be done, that further evaluation is considered.

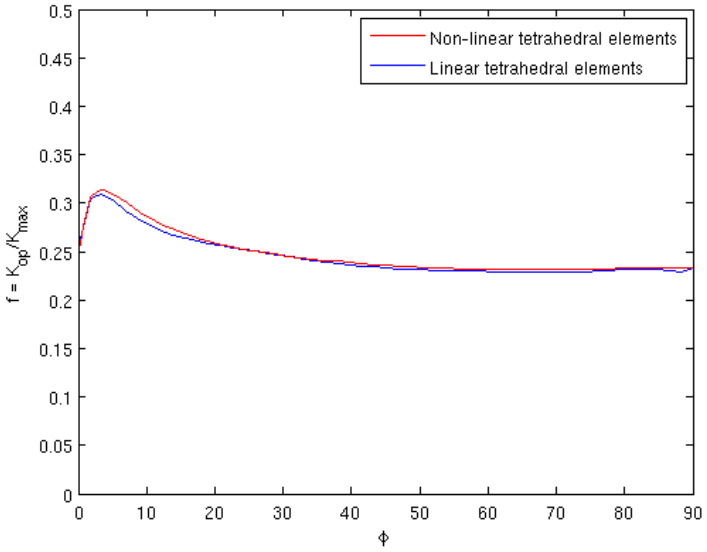

Figure C.5: Comparison of the closure levels along the crack front using linear tetrahedral elements and quadratic tetrahedral elements in the transition zone.

Appendix D
– Extrapolation method of crack growth for stabilization

The blue curves in Figure D.1 (a) and (b) compares the closure level at the free surface ($\varphi = 0^o$) and at the mid plane ($\varphi = 90^o$) respectively. It is obvious that more nodes need to be released to achieve stabilized values at the free surface, where the stress gradient is larger. It would cause a huge computational effort if stabilized values were strictly to be found at all the degrees, however, since the final opening level determined is calculated as a weighted average of all degrees at the crack front, it has a minor effect of not fully capture the opening level at a few degrees.

An estimate of stabilized closure levels is otherwise desired but are sometimes difficult to obtain, for example when the initial forward plastic zone is large compared to the element size, i.e. a lot of nodes need to be released to establish a stabilized closure level. An interesting alternate method to establish stabilized values, although never used in this thesis, could be an extrapolation model of the form:

$$\frac{K_{\mathrm{op}}}{K_{\max}} = C_0 + C_1 * e^{C_2 * \Delta a^{C_3}} \tag{D.1}$$

This model proposed by Rodriguez [13] contains 4 fitting parameters. Consider Figure D.1 (a); at mid plane the opening level seems to be stabilized after letting the crack propagate about 18-20 elements (i.e. 18-20 load cycles applied), but in D.1 (b) crack has not grown far enough to provide steady state values. Figure D.2 (a) also presents extrapolated values by using one, two, three to twenty crack increments as a test to find how many nodes are needed in order for the extrapolation model be valid and give values corresponding to the numerical results. It seems, from this test, that the model converges after using around 12 values for the curve fitting. In this case, only 12 cycles with corresponding number of node released would have been enough if used in combination with this extrapolation model. To get a better estimate of the opening level at zero degrees, where the opening levels has not yet converged for 20 node released as in D.1 (b), this method provides a value of $\frac{K_{\mathrm{op}}}{K_{\max}} =$ 0.4. All previous 20 values were used in the curve fitting and then extrapolated for convergence. Although, a converged result is not established until an unrealistic number of nodes are released

(around 250), the value itself can be considered to be reliable.

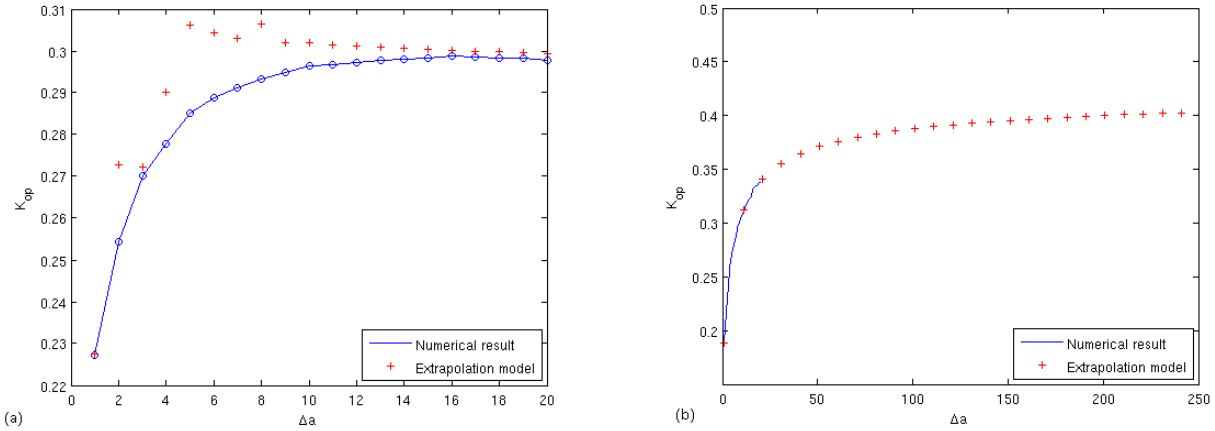

Figure D.1: R = 0, L_e = 0.005 mm, T = 20 °C . Closure levels at (a) mid plane ($\phi = 90^0$) and at (b) the free surface ($\phi = 0^0$). (a) also demonstrates how many increments that is needed for steady state behavior by use of Rodriguez extrapolation equation, (b) shows the effect of using Rodriguez extrapolation equation for 250 increments at the free surface where stabilized closure levels are more difficult to establish.